



Review

# Strategic Development of Piezoelectric Nanogenerator and Biomedical Applications

Omkar Y. Pawar <sup>1,2,3</sup>, Snehal L. Patil <sup>1,2</sup>, Rahul S. Redekar <sup>2</sup> , Sharad B. Patil <sup>1,4</sup>, Sooman Lim <sup>3,\*</sup>   
and Nilesh L. Tarwal <sup>2,\*</sup>

<sup>1</sup> School of Nanoscience and Technology, Shivaji University, Kolhapur 416004, Maharashtra, India

<sup>2</sup> Smart Materials Research Laboratory, Shivaji University, Kolhapur 416004, Maharashtra, India

<sup>3</sup> Graduate School of Flexible and Printable Electronics, Jeonbuk National University, 567 Baekje-daero, Deokjin-gu, Jeonju 54896, Republic of Korea

<sup>4</sup> Center for Interdisciplinary Research, D.Y. Patil Education Society (Deemed to be University), Kasaba Bawada, Kolhapur 416006, Maharashtra, India

\* Correspondence: smlim@jbnu.ac.kr (S.L.); nlt.phy@unishivaji.ac.in (N.L.T.)

**Abstract:** Nanogenerators are the backbone of self-powered systems and they have been explored for application in miniaturized biomedical devices, such as pacemakers. Piezoelectric nanogenerators (PENGs) have several advantages, including their high efficiency, low cost, and facile fabrication processes, which have made them one of the most promising nano power sources for converting mechanical energy into electrical energy. In this study, we review the recent major progress in the field of PENGs. Various approaches, such as morphology tuning, doping, and compositing active materials, which have been explored to improve the efficiency of PENGs, are discussed in depth. Major emphasis is given to material tailoring strategies and PENG fabrication approaches, such as 3D printing, and their applications in the biomedical field. Moreover, hybrid nanogenerators (HNG), which have evolved over the last few years, are discussed. Finally, the current key challenges and future directions in this field are presented.

**Keywords:** nanogenerator; piezoelectric; perovskite; hybrid materials; self-powered; bio-sensors



**Citation:** Pawar, O.Y.; Patil, S.L.; Redekar, R.S.; Patil, S.B.; Lim, S.; Tarwal, N.L. Strategic Development of Piezoelectric Nanogenerator and Biomedical Applications. *Appl. Sci.* **2023**, *13*, 2891. <https://doi.org/10.3390/app13052891>

Academic Editor: Antonio Di Bartolomeo

Received: 13 January 2023

Revised: 13 February 2023

Accepted: 13 February 2023

Published: 23 February 2023



**Copyright:** © 2023 by the authors. Licensee MDPI, Basel, Switzerland. This article is an open access article distributed under the terms and conditions of the Creative Commons Attribution (CC BY) license (<https://creativecommons.org/licenses/by/4.0/>).

## 1. Introduction

Advances in technology have enabled researchers to miniaturize electronic components and develop portable devices, such as mobile phones, laptops, and smartwatches. The miniaturization of electronic devices is inevitable in the development of modern technologies to ease operations in almost all sectors. Sectors such as the bio-implants sector rely heavily on miniaturized devices, such as pressure sensors, pacemakers, and nerve stimulators [1–3]. These bio-implant devices require external power for their proper functioning. Utilizing batteries to power these microdevices is not a practical approach as their size is considerably small compared with the currently developed batteries. The development of self-powered systems that can harvest energy from various sources from their surroundings to power these micro-implants is a significant breakthrough in addressing this limitation [4]. Thus, battery problems, such as their limited cycle life and large size and the need for frequent maintenance, can be resolved using self-powered systems. Nanogenerators are well-known examples of self-powered systems that can harvest different forms of energy [5]. Research on nanogenerators has evolved exponentially over the past few decades. Depending on the form of energy conversion, nanogenerators can be classified as piezoelectric nanogenerators (PENGs), triboelectric nanogenerators (TENGs), or pyroelectric nanogenerators (PYNGs) [6–8]. PENGs are promising candidates owing to their high efficiency, low cost, facile fabrication techniques, and wide range of applications.

PENGs work on the basis of the piezoelectric effect, also referred to as the direct piezoelectric effect, which is a unique property of a material that generates an electric

field when subjected to mechanical stress. Piezoelectric materials are non-centrosymmetric materials that experience electric polarization under external mechanical stress. For example, ZnO has  $\text{Zn}^{2+}$  cations and  $\text{O}^{2-}$  anions stacked layer by layer in a crystal structure; in an undisturbed state, the charge centers of the cation and anion coincide with each other. When external stress is applied to the crystal, structural deformation occurs and the charge centers are displaced. The separation of charge centers generates polarization, and when an external load is connected to the crystal, the electrons begin flowing from the external circuit to achieve a new equilibrium. Thus, mechanical energy is converted to electrical energy [9]. This phenomenon is reversible; when an electrical field is applied to the piezoelectric material, a change in dimension can be observed owing to the generation of internal stress [10]. Based on their structure, PENGs can be classified into three types: vertical-nanowire integrated nanogenerators (VINGs), lateral-nanowire integrated nanogenerators (LINGs), and nanocomposite electrical nanogenerators (NEGs).

In 2006, for the first time, Wang et al. [11] fabricated a VING utilizing vertically aligned ZnO nanorods and reported an efficiency of 17%–30%. In 2007, Price et al. [12] developed a fully operational VING device comprising ZnO nanowires underneath a zigzag metal electrode to harvest the energy from ultrasonic waves. In 2008, Yang et al. [13] introduced a single-ZnO nanowire generator placed horizontally on a polyamide film, a flexible substrate, thereby generating potential by means of lateral bending. This model was further modified by adding multiple ZnO nanowires with a lateral alignment, referred to as LING. Subsequently, various approaches have been reported to fabricate LING. For example, Zhu et al. [14] demonstrated a unique fabrication technique, wherein vertically aligned ZnO nanorods, grown via physical vapor deposition, were transferred to another substrate to create horizontal nanorod alignment and generated a high output voltage (2.03 V). In 2010, Momeni et al. [15] introduced NEG, wherein PENG was developed as a nanocomposite, comprising ZnO nanorods in an epoxy matrix. The polymer matrix in the NEG provides good mechanical support for the piezoelectric nanostructure. In addition, the NEG offers higher output potential compared with VINGs and LINGs. To improve the efficiency of PENGs, researchers have explored novel materials, such as sodium bismuth titanates (BNTs) and graphitic carbon nitride ( $\text{g-C}_3\text{N}_4$ ), owing to their superior piezoelectric characteristics [16,17]. The piezoelectric response depends strongly on the morphology of the piezoelectric material; for example, ZnO nanosheets and nanodiscs demonstrate superior piezoelectric performance compared with ZnO nanorods [18,19]. To further improve performance, researchers have been developing new approaches, such as interfacial modifications and 3D printing techniques [20,21]. Recently, the concept of a hybrid structure has gained the attention of researchers as it can harvest energy, such as mechanical stress and heat simultaneously from multiple sources, thus drastically enhancing the device's performance [22]. However, these approaches have not yet been thoroughly discussed. Therefore, the recent developments in the field of PENGs must be summarized.

This review presents an in-depth summary of recent developments in PENGs. It compiles research on PENGs, including recent reports and different strategies, such as electrode modification, selective laser sintering (SLS), and direct ink writing (DIW), which are discussed in detail. Additionally, emerging hybrid structures and their evolution over the last few years are included. This article begins with different materials used in the fabrication process. More emphasis is placed on the different strategies that researchers have followed to improve output performance. Additionally, the potential applications of PENGs in biomedical fields are presented. Finally, we discuss the future outlook based on the knowledge acquired.

## 2. Piezoelectric Materials

Materials that can transform mechanical energy into electrical energy are referred to as piezoelectric materials. Piezoelectric materials lack a center of symmetry, which endows them with the unique property of converting mechanical deformations into elec-

trical energy; furthermore, materials with highly piezoelectric properties can enhance the performance of devices. Piezoelectric materials can be divided into various categories, such as single crystals, perovskite materials, and polymers. This section focuses on the different piezoelectric materials used for the fabrication of PENGs and their properties (Figure 1).

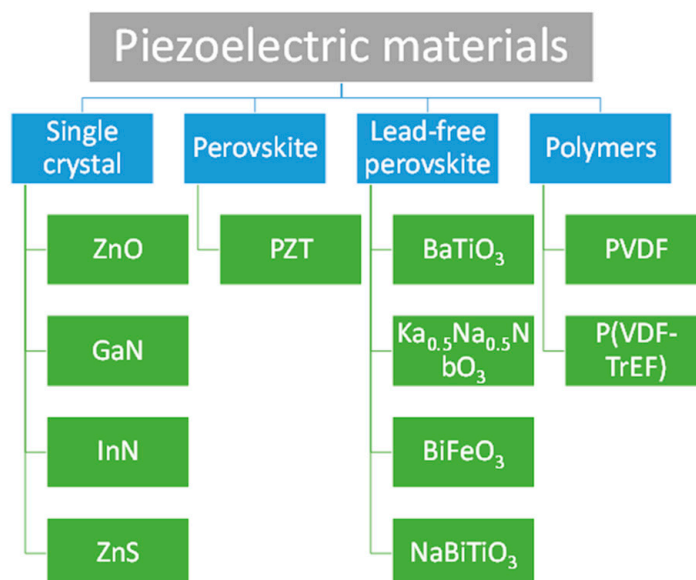


**Figure 1.** Different classes of piezoelectric materials and examples.

### 2.1. Single-Crystal Materials

The first class of piezoelectric materials contains single-crystal materials; ZnO, GaN, InN, and ZnS fall in this category and primarily exhibit a wurtzite structure. Among these, ZnO has been extensively explored for PENG applications owing to its availability and biocompatibility.

The first PENG was fabricated using ZnO nanowire arrays [11], which raised the problem of low output efficiency. Since then, numerous attempts have been made to enhance the output; for example, a PENG was built using a single nanowire laterally placed on a flexible substrate with both ends connected to the electrode. The nanowire was stretched by bending the flexible substrate to generate piezoelectric potential along the nanowire. The piezoelectric response was produced via periodic bending and relaxation of the nanowire in the form of an electric signal. Such a PENG based on a laterally grown single-ZnO nanowire generates an output voltage of 20–50 mV and a short-circuit current of 400–750 pA. A PENG based on laterally grown ZnO nanowires was employed to harvest energy from human motions, such as finger tapping and heartbeats [23].

Researchers introduced the VING and LING structures because of the low output performance of single-nanowire-based nanogenerators. The fabrication of VING and LING was achieved by integrating ZnO nanowire arrays vertically and laterally, respectively; thus, they are also referred to as integrated nanowire nanogenerators. Integrated nanowire PENGs produced a maximum open-circuit voltage and short-circuit current of 1.26 V and 28.8 nA, respectively [24]. Although the PENG with an array of ZnO nanowires was able to deliver a decent output, it was relatively low due to the poor piezoelectric characteristics of ZnO. This led to further research aiming to discover materials with good piezoelectric properties, namely, the piezoelectric coefficient and dielectric constant.

### 2.2. Perovskite

There are two classes of perovskite materials, lead-perovskite materials and lead-free perovskite materials.

### 2.2.1. Lead Perovskite Materials

After realizing the low performance of ZnO-based PENGs, researchers diverted their focus to lead zirconate titanate  $[\text{Pb}[\text{Zr}(x)\text{Ti}(1-x)\text{O}_3]]$  (PZT)-based ceramic materials. PZT ceramics exhibit good crystallinity, a high dielectric constant, and a high piezoelectric constant. These superior properties have attracted the attention of many researchers, thus resulting in tremendous developments in relation to PZT-based PENGs. PZT is highly piezoelectric; however, fabricating a thin film is laborious owing to its brittleness. The complex synthesis process and their brittle nature are major obstacles in the fabrication of PZT-based PENGs. Although researchers have made numerous attempts to overcome these obstacles by fabricating different morphologies and applying unique processes, the developments in PZT-based PENGs has dropped exponentially due to the hazardous nature of lead. Consequently, attention is now being paid to exploring lead-free perovskite materials in PENGs [25,26].

### 2.2.2. Lead-Free Perovskite Materials

Owing to the toxicity and hazardous nature of lead, researchers are now focusing on the application of lead-free perovskite materials for high-performance PENGs. Piezoelectric lead-free perovskite ceramics are generally polycrystalline materials consisting of irregular collective small grains and are typically prepared through solid-state reactions and sintering processes. The piezoelectric coefficient is governed by the phase transition temperature; the polarization vectors change their direction during the phase transition (tetragonal–orthorhombic/monoclinic, orthorhombic/monoclinic–rhombohedral), thus resulting in a higher piezoelectric coefficient [27].

Lead-free perovskite materials have the general molecular formula  $\text{ABO}_3$ , where cations A and B form a family of oxides represented as  $\text{A}^{\text{II}} \text{B}^{\text{IV}} \text{O}_3$ ,  $\text{A}^{\text{III}} \text{B}^{\text{III}} \text{O}_3$ , and  $\text{A}^{\text{I}} \text{B}^{\text{V}} \text{O}_3$ .

#### (I) $\text{A}^{\text{II}} \text{B}^{\text{IV}} \text{O}_3$

One of the most extensively used lead-free perovskite materials is barium titanate ( $\text{BaTiO}_3$  BTO). Studies have been conducted on BTO as a model material to investigate its ferroelectric and piezoelectric properties at the nanoscale [28,29]. In BTO, a phase transition occurs as the temperature decreases, and the phase transforms from tetragonal to orthorhombic, and eventually to rhombohedral [30,31]. In 2009, a BTO-based composite was reported as a high-performance piezoelectric material with a piezoelectric coefficient of  $d_{33} \approx 620 \text{ pc/N}$  [32]; additionally, a composite of barium zirconate titanate–barium calcium titanate  $0.5 \text{ Ba}(\text{Ti}_{0.8} \text{Zr}_{0.2})-(\text{Ba}_{0.7} \text{Ca}_{0.3}) \text{TiO}_3$  (BZT-BCT) exhibited a drastic enhancement in performance. The BZT-BCT nanowire synthesized via a two-step hydrothermal process exhibited an open-circuit voltage of 6.25 V and an overall power density of  $2.25 \mu\text{W}/\text{cm}^3$  [33]. To further enhance the performance, different strategies, such as morphological alterations, have been adopted. Numerous techniques, such as solvothermal synthesis [34], a molten salt method [35], and supercritical fluid technology [36], have been reported for the synthesis of BZT-BCT. Note that the piezoelectric properties of the bulk and nanomaterials differ significantly owing to the difference in their surface area-to-volume ratios [37].

Another promising material is BNT (also known as NBT:  $(\text{Na}_{1/2} \text{Bi}_{1/2}) \text{TiO}_3$ ), which exhibits a perovskite structure at room temperature. Herein, the phase transition from cubic to tetragonal and then to rhombohedral occurs as the temperature decreases from approximately  $540 \text{ }^\circ\text{C}$  to  $300 \text{ }^\circ\text{C}$  [38]. NBTs have strong ferroelectric properties, with high remnant polarization ( $\text{Pr} = 38 \mu\text{C}/\text{cm}$ ), and several relaxer ferroelectric (ferroelectric materials that exhibit high electrostriction) NBT-based compositions have high piezoelectric coefficients; these have been used to fabricate high-performance lead-free PENGs. NBT materials exhibit shallow depolarization temperatures and significant leakage current values, which are major drawbacks of these materials [39].

## (II) $A^{III}B^{III}O_3$

A well-known example of an  $A^{III}B^{III}O_3$ -type lead-free perovskite material is bismuth ferrite ( $BiFeO_3$ , BFO) [40]. BFO is a piezoelectric material that exhibits a high Curie temperature (approximately 809 °C–830 °C); thus, it is a suitable candidate for high-temperature applications [41,42]. In particular, BTO and  $PbTiO_3$  were alloyed with BFO to achieve rhombohedral and tetragonal phase boundaries, which improved the piezoelectric response [43]. BFO has the unique property of being magnetic and strongly ferroelectric at room temperature [44,45]. It is the most promising candidate for enhancing or modifying the ferroelectric properties of BTO and  $SrTiO_3$  solid-solution systems [45].

## (III) $A^IB^VO_3$

The key advantages of the typical  $A^IB^VO_3$  class are its Curie temperature ( $T_C = 420$  °C) [46], good ferroelectric properties, with remnant polarization of  $P_r = 3.3$   $\mu C/cm^2$  [47], as well as its excellent electrochemical coupling factors. Owing to these properties,  $A^IB^VO_3$  materials are widely used as lead-free piezoelectric materials; furthermore, these materials are eco-friendly and biocompatible [48]. Potassium sodium niobate (KNN) ( $K_xNa_{1-x}NbO_3$ ) is commonly used for PENG applications. The phase transition of pristine KNN occurs from cubic (paraelectric) to tetragonal to orthorhombic, and finally to rhombohedral (ferroelectric); the KNN orthorhombic phase is typically observed at room temperature [49]. Various KNN morphologies have been reported in the literature, including nanoparticles [50], nanotubes [51], nanofibers [52], and nanopellets, which have been obtained using different physical and chemical synthesis methods.

### 2.3. Polymer Materials

Single-crystal and perovskite materials are not flexible; therefore, polymer materials are often incorporated into PENGs. After the discovery of the polyvinylidene fluoride (PVDF) polymer, the applications of piezopolymers in sensors and actuators [53] have considerably increased owing to their excellent flexibility, low production cost, and fast synthesis compared with most piezoelectric materials [54]. The good biocompatibility of polymers, such as PVDF and polyvinylidene fluoride trichloroethylene P(VDF-TrFE), makes them promising candidates for piezo-biomedical applications [55]. Piezo-polymers are classified as bulk, void-charged, and composites [56]. Void-charged polymers are composed of thin layers with gas voids that generate internal dipoles on charging, which is essential for the piezoelectric effect. By contrast, bulk polymers are semi-crystalline polymers. For example, PVDF is a bulk semicrystalline polymer with five crystalline phases— $\alpha$ ,  $\beta$ ,  $\gamma$ ,  $\delta$ , and  $\epsilon$ —among which  $\alpha$  and  $\beta$  are highly piezoelectric [57]. Numerous studies have been reported on the fabrication of flexible PENGs.

In the present section, different classes of piezoelectric materials, such as single crystals, perovskites, and polymers, were summarized. Every material has its own characteristic properties in terms of its piezoelectric response, synthesis process, flexibility, and biocompatibility. Thus, appropriate materials are selected according to the application requirements.

## 3. Strategies

Analyzing the performance of the fabricated device is an essential aspect of research. Research on the fabrication of PENGs with high yield and low production costs has been conducted extensively. Different techniques, such as doping, tailoring of the morphologies of materials, using multiple substrates, fabricating thin-film composites by means of 3D printing techniques, electrode modification, interfacial modification, and fabricating hybrid structures, have been applied to enhance PENG performance. In this section, we provide a brief overview of the various strategies investigated thus far (Figure 2).

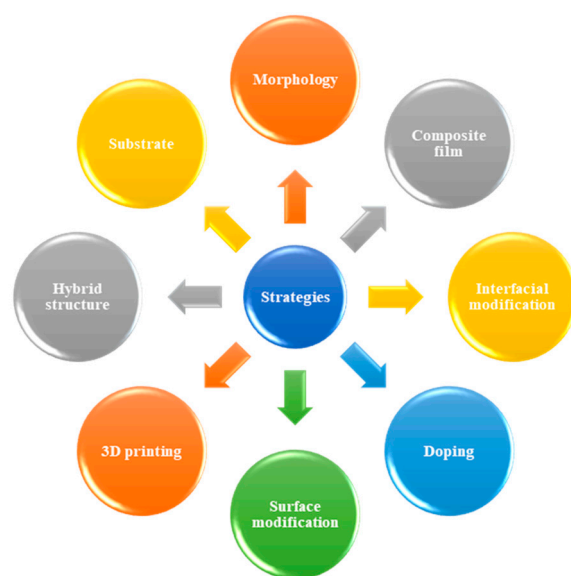


**Figure 2.** Different strategies used to improve the performance of PENGs.

### 3.1. Effect of Morphology

The morphology of a piezoelectric material has a substantial impact on piezoelectric performance, and the desired properties can be achieved by tuning the morphology of the material. Different reaction parameters, such as the reaction temperature, concentration, and pH, influence the morphology of the material [58–60]. Nanostructures formed with different morphologies, such as nanowires, nanoribbons, nanotubes, nanorods, and nanopillars, exhibit different properties.

ZnO nanostructures are widely utilized in the fabrication of PENGs because of their chemical stability, biocompatibility, and low cost [61]. ZnO is a potential candidate for PENGs owing to its good piezoelectric response, its availability, and its economical fabrication processes. Nonetheless, ZnO suffers from several difficulties, primarily the screening effect, which hinders its piezoelectric performance. Several strategies have been introduced to minimize these problems and enhance the performance of ZnO-based nanogenerators. Fabricating different morphologies is considered an excellent approach in improving the performance of PENGs.

ZnO can be fabricated with different morphologies to achieve desired properties; for example, ZnO nanorods exhibit better performance compared with ZnO nanowires. Zhu et al. [14] demonstrated a unique fabrication technique, wherein vertically aligned ZnO nanorods, grown on Si substrate via physical vapor deposition, were transferred to another substrate to create a horizontal nanowire array. They have used a mechanical setup to transfer the nanowire on a resaving substrate shown in Figure 3A(a). Figure 3A(b) shows the SEM image after the transfer process. The receiving substrate was swept across the vertically aligned ZnO nanowire in a counterclockwise direction due to which the nanowire gets detached from the Si substrate and gets horizontally aligned on the receiving substrate. The fabricated device generated an output voltage of 2.03 V with a current of 107 nA. Reportedly, nanogenerators based on high-density, well-aligned ZnO nanorods with decent crystal quality generated an output voltage of 9.5 mV [62]. A nanogenerator based on a laterally grown ZnO nanowire array fabricated via 3D printing generated an output voltage of 2.03 V [11]. Two-dimensional (2D) morphologies, such as ZnO nanodiscs, have been recently developed, and nanogenerators based on ZnO nanodiscs deliver a DC output voltage of 17 V with a current density of 150 nA/cm<sup>2</sup> under vertical compressive strain [19]. Another example of the 2D ZnO nanostructure is the nanosheet, which is an attractive morphology. A high surface-to-volume ratio and good durability under repetitive mechanical damping make ZnO nanosheets a promising candidate for application in PENGs. Kim et al. [18] fabricated a PENG based on ZnO nanosheets, considering the

drawbacks of 1D nanostructure-based PENGs (the occurrence of fractures when the critical force limit was exceeded). The authors fabricated a 2D ZnO nanosheet-based PENG which was able to produce high output performance without any degradation. The device was fabricated in a stepwise manner. In the first step, the ZnO nanosheets were grown on an Al substrate via an aqueous solution route. Then, in the next step, the Au layer was deposited on a polyethersulphone substrate. The exact structure of the device is shown in Figure 3B(a). The authors demonstrated the effect of the buckling of nanosheets and ionic layer coupling, which were able to provide an efficient DC output. They recorded an output voltage of 0.5 V and a current density of  $15 \mu\text{A}/\text{cm}^2$ . Figure 3B(b,c) shows the switching polarity of the fabricated device under 4.0 kgf. Recently, a PENG based on ZnO nanoflakes with a thickness of 10 nm was synthesized via a novel synthetic route, generating a peak-to-peak open-circuit voltage of 127 V and a short-circuit current of  $80 \mu\text{A}$ . An immense output power density of  $1.2 \text{ mW}/\text{cm}^2$  was achieved for the PENG based on ZnO nanoflakes [63].

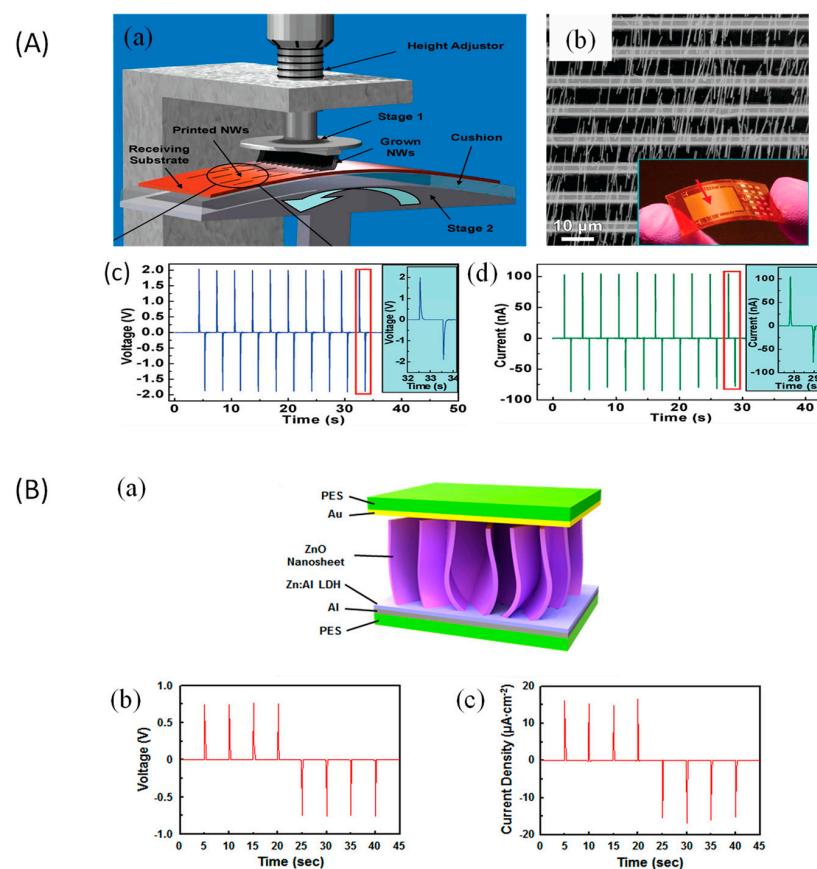


**Figure 3.** (A) Fabrication and characterization of the HONG device. (a) Schematics of the experimental setup used for transferring the vertically aligned ZnO nanowire onto a flexible substrate by changing their alignment to horizontal. (b) SEM image of horizontally aligned ZnO nanowire with an Au electrode printed on it (sputtering). Inset: actual photograph of the fabricated device. (c) Open-circuit voltage of HONG. (d) Short-circuit current of HONG. Both (c,d) were obtained under 0.1% strain, at a  $5\% \text{ s}^{-1}$  strain rate, with a deformation frequency of 0.33 Hz. The enlarged view of the red box was shown in the inset. The inset shows an enlarged view of deformation cycles. Reprinted with permission from [14]. Adapted with permission from Zhu et al. (2010). Copyright © 2010 American Chemical Society. (B) Two-dimensional nanosheets/ionic layer heterojunction-based PENG. (a) Schematics of 2D nanosheet-based PENG, with 2D nanosheets and an anionic nanoclay layer heterojunction. (b,c) depict the output voltage and output current density, respectively, in the switching-polarity test at 4 KgF [18]. Adapted with permission from Kim et al. (2013). Copyright © 2013 *Nature*.

PZT can also be synthesized with various morphologies, such as crystalline nanowires, nanorods, and nanofibers. An energy harvesting device fabricated with a single-crystal PZT nanowire [64] generated an output voltage of 10 V under specific applied pressure, whereas nanorods of PZT delivered an output voltage of 3.3 and 8 V under a compressive force of 10 N and a continuous tapping motion, respectively. At 10 N compressive forces, the device demonstrated a power density of  $3.16 \mu\text{W}/\text{cm}^2$  and  $5.12 \mu\text{W}/\text{cm}^2$  under 10 N and a continuous tapping motion [65]. Qi et al. [66] fabricated a PENG based on PZT nanoribbons. They fabricated a flexible PDMS/PZT nanoribbon-based device (shown in Figure 4a) using a stepwise fabrication process. In the first stage, PZT nanoribbons were prepared by means of a standard sputtering process on a MgO substrate. Subsequently, the substrate was undercut and etched, and the PZT nanoribbons were transferred to polydimethylsiloxane (PDMS) gel silica. The fabricated device was examined using a piezoelectric force microscope. The device delivered an open-circuit voltage and a short-circuit current of 0.25 V and 40 nA, respectively. Figure 4d shows the results of measurements in which charge density and pressure oscillated in phase, comparing the  $d_{31}$  values obtained after and before poling, which were 49 pm/V and 79 pm/V, respectively. In another study, a PENG based on a PZT large-area thin film was prepared using the laser lift-off (LLO) process; the entire area of the PZT thin film was transferred onto the flexible substrate without any mechanical damage using laser radiation. The fabricated device produced an output voltage of 200 V and a current of  $150 \mu\text{A}/\text{cm}^2$  under periodic bending and releasing motions [67]. Zhang et al. [68] fabricated a PENG using PZT nanowires with a unique layered nanostructure, which was synthesized via a hydrothermal method. The nanowires were grafted onto the PDMS polymer to form a composite. The fabricated device generated an output voltage of up to 2.7 V, with a power density of  $51.8 \mu\text{W}/\text{cm}^2$ . These output voltage characteristics were observed at its fundamental resonance (25.2 Hz) under a root mean square acceleration input of 0.1 g. Although PZT-based materials provide excellent performance, the lead content in PZT is a key concern. Lead is a highly toxic material and has numerous adverse effects on the environment. To overcome this drawback, researchers have shifted their focus to implementing lead-free perovskite materials in PENG.

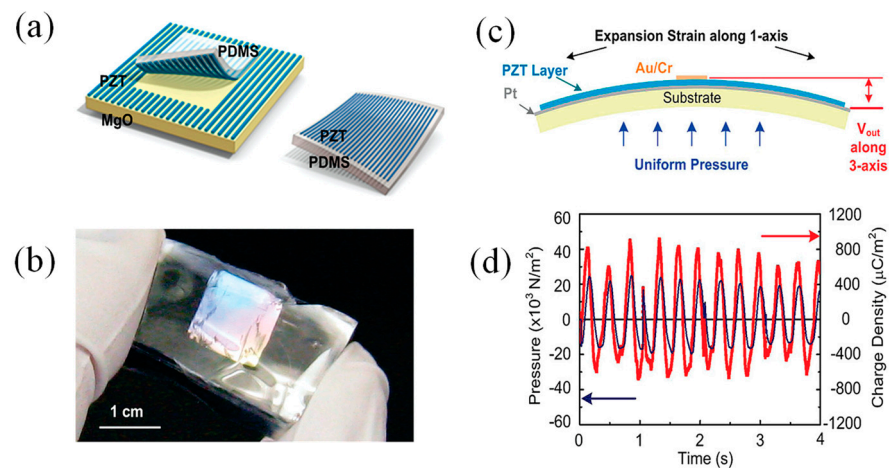


**Figure 4.** Transfer of PZT nanoribbons from an MgO substrate to a flexible rubber substrate. (a) Crystalline PZT ribbons are synthesized on an MgO host substrate, which is subsequently etched, and the ribbons are transferred and printed onto flexible PDMS rubber. (b) Photograph of a piece of PDMS with PZT ribbons covering the top surface. (c) Schematic of a specimen indicating 31-mode piezoelectric bending and measurement. The PZT layer; top and bottom contact electrodes and substrate are indicated. (d) Oscillating pressure (left axis) and induced dielectric displacement (right axis) [66]. Adapted with permission from Qi et al. (2010). Copyright © 2010 American Chemical Society.



Several lead-free perovskite materials, such as BTO, BFO, KNN, and BNT, are available. BTO is a popular perovskite lead-free material used for the fabrication of PENGs. BTO can be synthesized to form various morphologies, such as nanotubes, nanowires, and nanopillars [69]. The morphologies of the fabricated materials strongly influence their piezoelectric properties, such as energy conversion and efficiency. Reportedly, a nano-generator based on BTO nanotubes composited with PDMS was used to form a transparent device (shown in Figure 5A(a)). The BaTiO<sub>3</sub> nanotubes were synthesized via the hydrothermal method. In Figure 5A(b,c) one can observe the randomly oriented BaTiO<sub>3</sub> nanotubes in the PDMS matrix. The fabricated device generated an output voltage of 5.5 V and a short-circuit current of 350 nA [70]. This device was used to drive a commercial light emitting diode (LED) display. Compared with nanotubes, the BTO nanowire/PDMS composite-based nanogenerator exhibited slightly enhanced performance. A device based on BTO nanowires/PDMS nanocomposite delivered an output voltage of approximately 7.0 V, with a current of 360 nA [71]. Chen et al. [72] fabricated a PENG based on the BTO micropillar morphology. A P(VDF-TrFE)/BTO micropillar composite was synthesized via the sol-gel method, and it was polarized under a high electric field and ultraviolet (UV) light. The P(VDF-TrFE)/micropillar composite-based PENG exhibited an enhanced output voltage of 13.2 V with a current density of 0.33  $\mu\text{A}/\text{cm}^2$ . In addition to nanorods, nanowires, and nanopillars, the unique morphology of BTO nanofibers was also investigated. The BTO-powder-incorporated PDMS matrix demonstrated an output current of 1  $\mu\text{A}$  and an open-circuit voltage of approximately 12 V [73].

Other lead-free perovskite materials, such as BFO, KNN, and NBT, have also been utilized in different morphologies. Raj et al. [16] introduced an NBT-based lightweight nanogenerator. In their work, NBT with a one-dimensional (1D) morphology was synthesized via a solid-state reaction. The piezoelectric composite (polycaprolactone/NBT nanoparticles) was prepared using the casting technique. The composite film was sliced. Subsequently, a gold (Au) layer was sputtered and copper wires were attached to the film using silver (Ag) paste. Then, a Kapton layer was attached to both sides of the composite film. The final operational PENG device provided an output voltage and current of 22 V and 140 nA, respectively, under an applied compressive force of 6 N. KNN can be formed in different morphologies. Bairagi et al. [74] fabricated a PENG based on KNN nanorods with a high aspect ratio (8.5). A hydrothermal method was used to synthesize the KNN nanorods, and a KNN nanorod/PVDF fibrous web was prepared via electrospinning (Figure 5B(a)). Aluminum (Al) tape was affixed to the fibers, which acted as the top and bottom electrodes (Figure 5B(b)). The fabricated device provided an open-circuit voltage of 23.24 V and a short-circuit current of 9  $\mu\text{A}$ . The KNN nanotubes exhibited a superior output current compared with the KNN nanorods [75].

The above description of different piezoelectric materials provides a brief overview of how the morphologies of the materials affect the output performance of the fabricated device, and some examples are mentioned in Table 1. As the active surface area increases, the stress distribution improves, thus enhancing the piezoelectric response. The performance of the same material varies with different morphologies; for example, ZnO nanoflakes generate a better response compared with other morphologies (nanowires, nanorods, and nanodiscs). Several unique morphologies have been reported to improve the performance of PENGs.

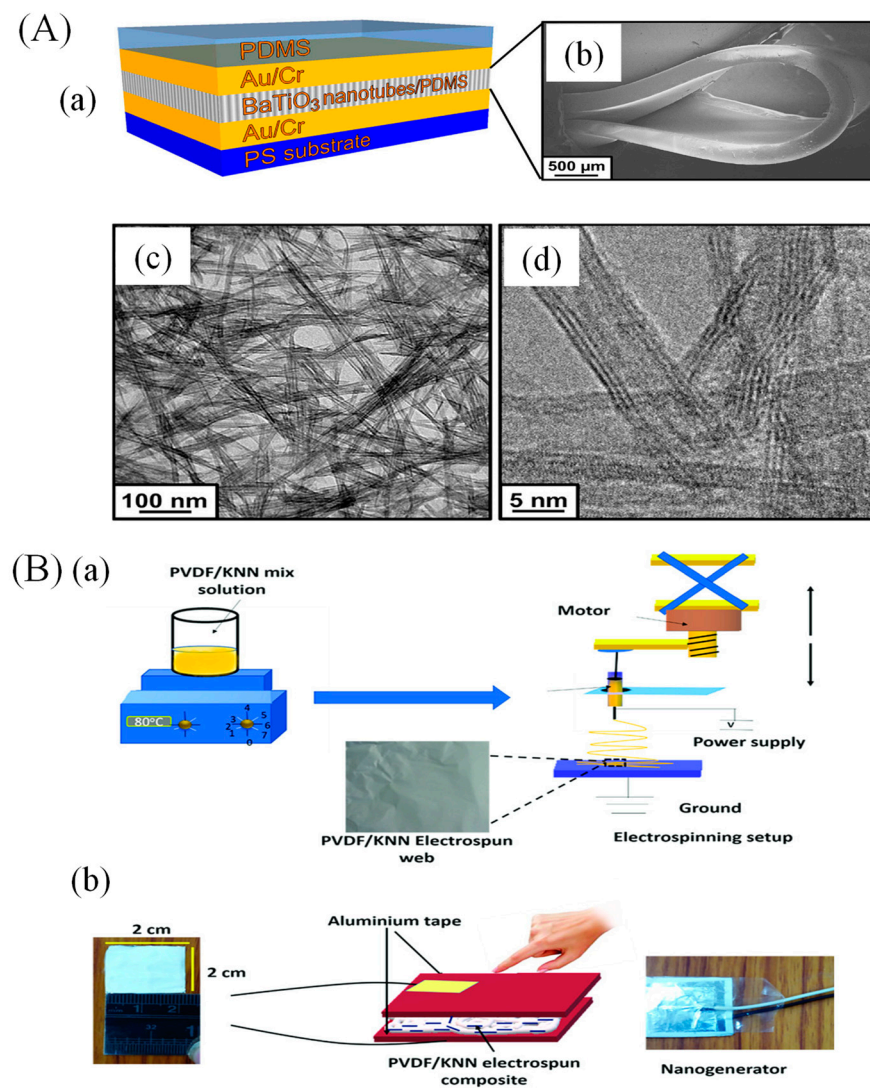


**Figure 5.** (A) BaTiO<sub>3</sub>-based flexible and transparent nanogenerator. (a) Schematics of the as-developed BaTiO<sub>3</sub>-based PENG. (b) SEM image of BaTiO<sub>3</sub> nanotube/PDMS composite. (c) TEM image of the synthesized BaTiO<sub>3</sub> nanotubes. (d) High-resolution TEM image of synthesized BaTiO<sub>3</sub> nanotube [70]. Adapted with permission from Lin et al. (2012). Copyright © 2012 American Chemical Society. (B) (a) Fabrication of PVDF/KNN NR film via the electrospinning method. (b) Fabrication of PVDF/KNN NR nanocomposite-based PENG [75]. Reprinted with permission from Bairagi and Ali. (2019). © 2019 WILEY-VCH Verlag GmbH and Co. KGaA, Weinheim.

**Table 1.** Some examples of piezoelectric materials with their different morphologies.

Sr. No	Material	Morphology	Synthesis Method	Operation Temperature	Output Voltage (V)	Output Current	Power Density	Ref.
1.	ZnO	Nanowire	Physical vapor deposition	150 °C	2.03	107 nA	11 mW/cm <sup>3</sup>	[14]
		Nanodisc	Seed-assisted solution route	150 °C	17	150 nA/cm <sup>2</sup>	-	[19]
		Nanorod	Chemical vapor deposition	95 °C	9–9.5	-	-	[62]

Table 1. Cont.

Sr. No	Material	Morphology	Synthesis Method	Operation Temperature	Output Voltage (V)	Output Current	Power Density	Ref.
2.	PZT	Nanoflake	Aqueous precipitation method	Room temperature	110	67 $\mu\text{A}/\text{cm}^2$	-	[63]
		Nanowire	Leaser lift off (LLO)	-	200	150 $\mu\text{A}/\text{cm}^2$	17.5 $\mu\text{W}/\text{cm}^2$	[67]
		Nanorod	Hydrothermal	180 °C	8	-	5.90 $\mu\text{W}/\text{cm}^2$	[65]
		Nanoribbons	Sputtering/dry transfer	-	0.25	40 nA	-	[66]
3.	BaTiO <sub>3</sub>	Nanotubes	Hydrothermal	200 °C	5.5	350 nA	-	[70]
		Nanowire	Hydrothermal	200 °C	7.0	360 nA	-	[71]
		Nanopillar	Nanoimprinting process	60 °C	13.2	0.33 $\mu\text{A}/\text{cm}^2$	-	[72]
4.	BNT	Nanoparticles	Solid State reaction	800 °C	22	140 nA	-	[74]
5.	KNN	Nanorods	Hydrothermal	160 °C	17	0.522 $\mu\text{A}$	9.135 $\mu\text{W}$	[75]

### 3.2. Doping and Compositing

In addition to tuning the morphology, doping and compositing are considered potential approaches to improve the piezoelectric performance. PENGs based on materials such as ZnO, PZT, lead-free perovskite materials, and polymers exhibit excellent piezoelectric outputs; however, the generated outputs are insufficient for conventional applications. The significant advantages of doping and compositing are that they increase the piezoelectric coefficient and the dielectric constant; additionally, compositing with a polymer can provide good flexibility and stretchability, which ultimately improves the output performance and durability. In the previous section, we provided an overview of the effect of morphology on the piezoelectric performance of materials, and in this section we summarize the effect of different dopants and composite materials on piezoelectric performance.

#### (I) ZnO

As discussed above, ZnO is the most extensively used piezoelectric material in PENG applications and it provides excellent output performance. The piezoelectric performance of ZnO-based PENGs can be further improved using appropriate dopants; *p*-type and *n*-type dopants are used. Doping ZnO with *p*-type dopants has been considered the simplest approach for enhancing the piezoelectric output. *p*-type doping can enhance electron transport by reducing the shielding effect on the electrons generated in the ZnO nanowires, whereas *n*-type doping induces lattice strain along the polar axis. The ionic radius of the dopant is an important factor to consider while doping the piezoelectric host material. If the dopant radius is too large or the concentration is too high, more lattice defects are generated, which affect the charge transport in the external circuits and decrease the output voltage. Some examples of dopants used for ZnO are halogen group elements, namely, iodine ( $\text{I}^-$ ), bromine ( $\text{Br}^-$ ), chlorine ( $\text{Cl}^-$ ), and fluorine ( $\text{F}^-$ ). Metal dopants including copper ( $\text{Cu}^{2+}$ ), cerium ( $\text{Ce}^{3+}$ ), europium ( $\text{Eu}^{3+}$ ), gadolinium ( $\text{Gd}^{3+}$ ), magnesium ( $\text{Mg}^{2+}$ ), manganese ( $\text{Mn}^{2+}$ ), lanthanum ( $\text{La}^{3+}$ ), chromium ( $\text{Cr}^{3+}$ ), vanadium ( $\text{V}^{5+}$ ), yttrium ( $\text{Y}^{3+}$ ), terbium (Tb), tin (Sn), and silver (Ag) [76–89], as well as nonmetallic dopants such as sulfur (S) [5], have also been used to explore the effect of doping on output voltage, as shown in Figure 6.

$\text{F}^-$  is the least used among the halide groups because its radius is smaller than that of oxygen ions, which hinders the output performance by inducing compressive strain within the crystal structure. However, the other halide dopants have a radius larger than the oxygen ion, and the generation of expansion strain along the *c*-axis of the ZnO lattice

results in the improved piezoelectric performance of the device. In the case of I<sup>-</sup>, the ionic radius is much larger than that of the oxygen ion, which results in distortion of the lattice structure and decreased piezoelectric performance. For instance, Rafique et al. [90] fabricated a PENG based on Br-doped ZnO nanosheets; in their work, ZnO nanosheets were synthesized via the facile hydrothermal method. The fabricated devices generated an output voltage of 8.82 V, which is greater than that of undoped ZnO nanosheets. Br<sup>-</sup> doping reduces the screening effect on the 2D nanosheets, which improves the performance of the fabricated device. Recently, Alnajar et al. [91] fabricated a piezoelectric sensor based on Er-doped ZnO. In their work, they compared the performance of ZnO, Er-doped ZnO, Er-doped GO/ZnO (1:10), and Er-doped GO/ZnO (1:5). The different compositions were synthesized via the wet chemical method. After the successful fabrication of the materials, they analyzed their performance which was as follows: (70 V, 1.85  $\mu\text{A}/\text{cm}^2$ ), (80 V, 2.16  $\mu\text{A}/\text{cm}^2$ ), and (100 V, 2.47  $\mu\text{A}/\text{cm}^2$ ) for Er-doped ZnO, Er-doped GO/ZnO (1:10), and Er-doped GO/ZnO (1:5) nanocomposite-based NGs, respectively, under a periodic force of 0.21 kgf.

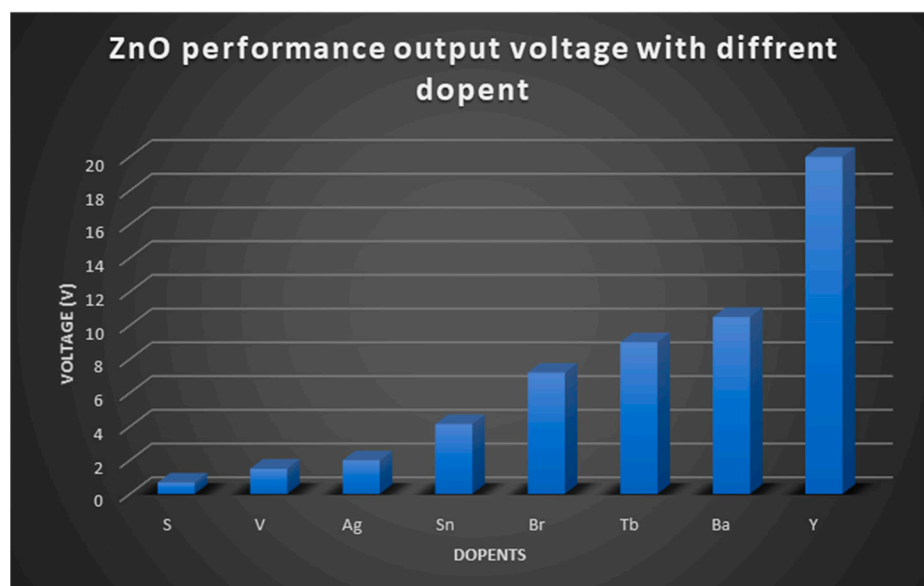


Figure 6. The output voltage of ZnO-based PENG with different dopants [5,76,86–89,91].

## (II) BTO

The piezoelectric performance of BTO can also be improved by selecting an appropriate dopant. Dopants, such as zirconium (Zr) [92] and tin (Sn) [93], can enhance the performance of BTO-based piezoelectric devices. Carbon-containing compounds are used as dopants to maintain a uniform distribution of BTO nanoparticles in polymers such as PDMS and PVDF.

In one study, BTO was doped with Zr; thus, the piezoelectric coefficient improved. Further, the  $\text{Ti}^{4+}$  ions were replaced with  $\text{Zr}^{4+}$  ions with smaller ionic radii, thus creating lattice distortion. The  $\text{TiO}_6$  octahedron of Zr-doped BTO doubled the piezoelectric performance compared with undoped BTO. Moreover, the peak-to-peak voltage and current of Zr doped BTO were observed to be 11.9 V and 1.35  $\mu\text{A}$ , respectively, which was more significant than undoped BTO (1.01  $\mu\text{A}$ ) [94]. Another example is Sn<sup>-</sup> and Ca<sup>-</sup>-doped PENGs. An Sn and Ca-co-doped BTO ( $0.82\text{Ba}(\text{Ti}_{0.89}\text{Sn}_{0.11})\text{O}_3-0.18(\text{Ba}_{0.7}\text{Ca}_{0.3})\text{TiO}_3$ ) material, synthesized via the freeze-drying method, generated an open-circuit output voltage of 39 V and a short-circuit current of 2.9  $\mu\text{A}$ , which were greater than those of Zr-doped BTO-based PENGs [95]. Thus, doping can remarkably improve piezoelectric properties, with unique mechanisms and outstanding performance.

### (III) Polymers

Many investigations have been carried out on polymers such as PVDF, P(VDF-HFP), etc. Doping is capable of improving the  $\beta$ -phase of the polymer, which improves the overall performance, as demonstrated in the following reports.

Adhikary et al. [96] investigated the effect of  $\text{Eu}^+$  doping on P(VDF-HFP)-based PENGs. In their work, they observed that  $\text{Eu}^+$  doping resulted in an improvement in the  $\beta$ -phase of more than 99%. In addition, they observed improved dielectric properties, which occurred due to the interaction between the O-H moieties of  $\text{Eu}^+$  and electronegative  $\text{CF}_2$  group of P(VDF-HFP). The fabricated device was able to deliver an open circuit voltage of 5 V with an open circuit current of 0.3  $\mu\text{A}$ . Garain et al. [97] fabricated PVDF/graphene-composite-based PENGs and investigated the effect of  $\text{Ce}^{3+}$  doping. The device was fabricated via the electrospinning method and had an excellent piezo-active  $\beta$ -phase without a post-pooling process. The fabricated device delivered an output voltage of 11 V, with a current density of 6  $\text{nA}/\text{cm}^2$ .

Apart from metallic dopants, carbon materials have also been utilized as dopants, improving the  $d_{33}$  value of the piezoelectric host and thereby improving the performance of the fabricated device. Carbon materials such as carbon nanotubes (CNTs) [98], graphene [99], and reduced graphene oxide (rGO) [100] act as conducting phases that improve the conduction network, which eventually elevates the piezoelectric performance. In addition, carbon materials reinforce mechanical properties [99]. Lou et al. [101] fabricated a PENG based on a BTO/PDMS composite using the easily modified solid-state method. The output performance was enhanced by doping acetylene black C with BTO; the  $d_{33}$  value increased from 5.4  $\text{pC}/\text{N}$  to 15.3  $\text{pC}/\text{N}$ . The PENG based on BTO/PDMS/C recorded an output voltage of 7.43 V when periodically beaten by the vibrator, and a 143% increment was observed compared with undoped BTO. Upadhyay et al. [93] fabricated a graphene-doped BTO/PVDF composite-based PENG using an electrospinning method. In their work, they compared the performance of PVDF, PVDF/BTO, and PVDF/BTO/graphene to determine the role of graphene doping. The PENG of PVDF with 0.15 wt% graphene and 15 wt% BTO generated an output voltage of 11 V. Recently Li et al. [100] fabricated a PENG based on rGO-doped BTO and investigated the effect of rGO doping on PVDF/BTO by comparing the output performance of rGO-doped PVDF/BTO and undoped PVDF/BTO. The undoped PVDF/BTO generated an open-circuit voltage of 4.65 V and short-circuit current of 1.82  $\mu\text{A}$ , whereas the rGO-doped PVDF/BTO provided a circuit voltage of 16.9 V and short-circuit current of 3.53  $\mu\text{A}$ . When the doping concentration exceeds a certain value, the composite turns into a conductor, and the piezoelectricity disappears.

Every piezoelectric material has drawbacks, such as low output, current loss, low flexibility, and high cost. The best way to overcome these problems is to combine different species with unique properties to achieve a trade-off. Typically, materials with flexibility and improved performance have been fabricated by compositing organic or inorganic polymers with different entities. Thin-film composites for PENGs are susceptible to the conversion of minimal mechanical action into electrical energy. Some examples are mentioned in Table 2.

**Table 2.** Examples of piezoelectric materials with different dopants.

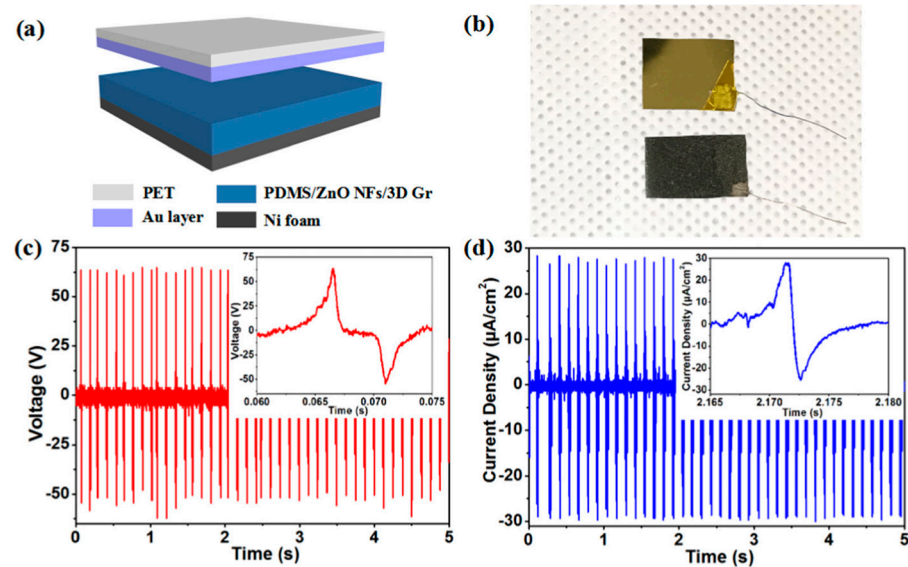
Material	Dopant	Morphology	Output Voltage		Output Current		Ref.
			(Undoped) (V)	(Doped) (V)	(Undoped)	(Doped)	
ZnO	S	Nanowire	0.659	0.689	49.7 $\text{nA}/\text{cm}^2$	57.3 $\text{nA}/\text{cm}^2$	[5]
ZnO	Cl	Nanowire	2.4	3.8	240 $\text{nA}/\text{cm}^2$	600 $\text{nA}/\text{cm}^2$	[76]
ZnO	Br	Nanowire	2.4	4.2	240 $\text{nA}/\text{cm}^2$	1000 $\text{nA}/\text{cm}^2$	[76]
ZnO	Y	Nanorods	-	20	-	-	[86]
ZnO	Sn	Nanorods	2.15	4.15	17 $\text{nA}$	36 $\text{nA}$	[87]
ZnO	Tb	Nanotaper	6.90	9	940 $\text{nA}$	-	[88]
ZnO	Ag	nanowire	0.5	2	200 $\text{nA}/\text{cm}^2$	500 $\text{nA}/\text{cm}^2$	[89]

Table 2. Cont.

Material	Dopant	Morphology	Output Voltage		Output Current		Ref.
			(Undoped) (V)	(Doped) (V)	(Undoped)	(Doped)	
BaTiO <sub>3</sub>	Zr doped	Nanocube	7.99	11.9	1.01 $\mu$ A	1.3 $\mu$ A	[94]
BaTiO <sub>3</sub>	Sn and Ca	-	-	2.9	-	2.9 $\mu$ A	[95]
BaTiO <sub>3</sub>	rGO	nanosphere	2.37	16.91	0.34 $\mu$ A	3.53 $\mu$ A	[100]
P(VDF-HEP)	Ag-doped	Nanofibers	1	3	0.3 $\mu$ A/cm <sup>2</sup>	0.9 $\mu$ A/cm <sup>2</sup>	[102]
P(VDF-HEP)	Eu <sup>3+</sup> -doped	Bilayer films	-	5.0	-	0.35 $\mu$ A	[96]
PVDF/Graphene	Ce <sup>+3</sup> -doped	Nanofiber	-	11	-	0.6 nA	[97]

The advantages of composite thin-film-based nanogenerators are that they provide low leakage current, high flexibility, easy large-scale fabrication, eco-friendliness, and robustness. Numerous polymers, such as P(VDF-HFP), PVDF, P(VDF-TrFE), PVC, and PDMS, [102–106] have been used to fabricate composite thin-film nanogenerators. A study on piezoelectric thin-film composites with BTO and organic polymers as active materials revealed that the piezoelectric performance was higher with organic polymers alone. This indicated that the PENG made of thin-film composite materials was able to fulfill the high-performance requirements and flexibility. Comparing the composite based on PDMS/BTO [106] and PVDF/BTO [99], the BTO nanoparticle/PDMS composite thin films delivered excellent performance. The nonpiezoelectric (PDMS)/BTO thin film, with uniformly distributed BTO in the polymer, formed a nondirectional polymer structure that improved the performance to a certain level. Lead-free materials are environmentally friendly and they provide an excellent piezoelectric response. BTO is the most widely used lead-free perovskite material in piezoelectric applications because of its ease of fabrication and the comprehensive investigations that have been conducted of its use in piezoelectric applications. Among the other lead-free perovskite materials with good piezoelectric properties, KNN is a promising candidate for PENG applications.

Xia et al. [107] demonstrated a novel approach towards fabricating a KNN-based PENG with enhanced performance; in their work, they incorporated a KNN/PDMS/C (C—acetylene black) composite into the device. They doped 12 wt% C, which resulted in a higher relative permittivity (173.56) and large remnant polarization (Pr, 1.84  $\mu$ C/cm<sup>2</sup>). A peak output voltage of 10.55 V was produced, which was 3.3 times higher than that of undoped KNN/PDMS. Qian et al. [108] reported a PNG device with Au as the top electrode and PDMS/Ni foam as the bottom electrode, where ZnO nanoflakes/graphene was incorporated into the PDMS as an active element (Figure 7a). This device powered 68 commercial LEDs, producing an output voltage of 122 V, with a current density of 51  $\mu$ A/cm<sup>2</sup> (Figure 7b,d). This excellent performance was due to three reasons: the flakes of ZnO provided a high active surface area, the 3D porous network of graphene provided a large surface area with an increased number of active sites for the growth of ZnO nanoflakes, and the PDMS layer functioned as a negative triboelectric material that reduced the screening effect. Tripathy et al. [109] developed a BFO-based piezoelectric nanogenerator. In their study, they fabricated a BFO copolymer P(VDF-TrFE)-based device, with BFO synthesized via a hydrothermal process. They fabricated two different films of BFO/P(VDF-TrFE) and BFO PVDF-HFP and compared the performance. They observed that the BFO/P(VDF-TrFE) film provided superior performance, and the 6 wt% BFO film improved the  $\beta$ -phase of the polymer. The fabricated device provided an output voltage of 18.5 V.



**Figure 7.** (a) Schematic structure of a PENG based on ZnO nanoflakes. (b) Image of an actual device. (c) Open-circuit voltage of PDMS/ZnO NF/3D Gr/Ni foam-based PENG. (d) Short-circuit current density of PDMS/ZnO NF/3D Gr/Ni foam-based PENG [108]. Reprinted with permission from Yang et al. (2018). Copyright © 2018 American Chemical Society.

### 3.3. Effect of Substrate

In addition to the different parameters mentioned above, the substrate also plays a vital role in the performance of PENGs. For example, Nour et al. [110] demonstrated the effect of two different substrates (plastic and paper) on a ZnO nanowire/PVDF nanohybrid on piezoelectricity. They conducted a comparative study on nanogenerators with plastic and paper substrates. The plastic- and paper-based devices provided an output voltage of 0.04 V and 4.8 V, respectively, thus suggesting that the paper substrate was more efficient than plastic; this was attributed to the porosity of the paper. Paper substrates can efficiently transfer pressure to the piezoelectric structure. These analyses demonstrated that porous and soft substrates have a greater tendency to act as efficient substrates. This suggests that the choice of substrate is crucial for the development of higher-performance nanogenerators.

### 3.4. Interfacial and Surface Modification

Improving the contact between the electrode surface and the piezoelectric nanostructure is another possible approach for improving piezoelectric performance. Interfacial modification is a unique strategy, wherein the output performance of a piezoelectric nanogenerator can be improved by enhancing the interfacial contact between the metal electrode and the active material. Designing a  $p-n$  junction or creating a Schottky contact between the metal electrode surface and the piezoelectric nanostructure are considered interfacial modifications. These two mechanisms can drastically improve performance by creating a built-in electrical field near the  $p-n$  junction, thereby reducing the carrier concentration and leakage current with the help of the Schottky barrier. Huan et al. [111] fabricated a PENG based on Ag/(KNN) heterojunctions, which improved the partial voltage applied to the KNN during the poling process and enhanced the performance of the fabricated device. The Ag/KNN heterojunction was created via photoreduction during KNN powder synthesis by means of a solid-state reaction. The KNN/multiwall (MW) CNT/PDMS piezoelectric film was prepared by mixing MW CNTs and KNN powder in the PDMS elastomer. The flexible device generated an open-circuit voltage of 240 V and short-circuit current of 23  $\mu\text{A}$ . Yin et al. [112] also reported the fabrication of an NiO-coated ZnO heterojunction with an increased DC output voltage of 430 mV, with an output current density of 40  $\text{nA}/\text{cm}^2$ . Liu et al. [113] also demonstrated an increase in the performance of ZnO-based PENGs using interfacial modification, but they combined this with doping. In their work, they fabricated

a device by doping ZnO with Cl, investigated the effect of different concentrations of Cl on performance, and compared the performance of the device with only interfacial modification and after doping. They observed a notable elevation in performance.

Nanoscale ZnO exhibits a large specific surface area due to quantum confinement effects. In some cases, piezoelectric performance is hindered by this high surface area. Due to quantum effects, aggregation occurs when the materials are composited with polymers such as PVDF-TrFE; furthermore, poor dispersion of the nanoparticles leads to low performance of the device. In such cases, surface modification is considered to be the best way to improve performance. Li et al. [114] demonstrated a unique path for the surface modification of ZnO nanoparticles. They utilized an *n*-propylamine (PA) dispersing agent and a silane coupling agent (1H, 2H, 1H, 2H, perfluorooctyltriethylesilane, PFOES). PA is a nonreactive agent that lowers the surface energy of ZnO nanoparticles but does not improve the interfacial binding between the particle surface and the polymer matrix. The output voltage of the fabricated ITO/P-Z-P-P/Au PENG was 24.4 % higher than that of the normal PENG.

### 3.5. Electrode Modification

Researchers have been developing new technologies. A new approach was introduced in which the electrode material was modified to improve the output performance. For instance, Zhang et al. [115] fabricated a PVDF niobate-based nanocomposite thin film; in their work, they fabricated flexible nylon nanofiber-supported Ag nanowires (NWs) with a network film as a flexible electrode. Gu et al. [20] developed a unique technique; they manipulated the electrode of a PENG. They introduced a unique design for a PENG based on a three-dimensional intercalation electrode. The intercalation-electrode-based nanogenerator, IENG, was fabricated using the spin-coating method. In the first step, a samarium-doped lead magnesium niobate nanowire (Sm-PMN-NW) composite was prepared via electrospinning. Second, a PDMS/Al electrode was fabricated. Third, the Sm-PMN-NW/PVDF composite was sandwiched between the bottom and top PDMS/Al electrodes. The PENG was constructed by stacking multiple layers of single PENG units formed as per the three steps described above. A boundary interface was created inside the piezoelectric material, thereby increasing the surface polarization charge. The IENG produced an output current of 320  $\mu$ A, which was 1.93 times higher than the previously recorded PENG value.

### 3.6. 3D Printing

3D printing is an additive manufacturing technique; it is well known for its ability to fabricate complex structures and it provides a simple bottom-up approach. 3D printing can be used to fabricate every part of a nanogenerator. There are various types of 3D printing, such as fused deposition modeling (FDA), SLS, stereolithography, and DIW, of which SLS and DIW are the most commonly used for the fabrication of PENGs. Song et al. [21] proposed a unique PVDF/graphene composite using the SLS method. They fabricated PVDF/graphene with enhanced piezoelectric properties. The fabricated device provided an open circuit voltage of 16.97 V and a short circuit current of 274 nA. Furthermore, the composite was able to produce sufficient energy to light 10 (LED) bulbs. Yang et al. [116] reported a PENG based on a PVDF/BTO/CNT composite (Figure 8b), with an improved  $d_{33}$  value and piezoelectric performance. A microporous wood-like structure was fabricated via SLS and supercritical carbon dioxide foaming (Figure 8a). The composite powder was prepared using a series of techniques including melt extrusion, granulation, low-temperature grinding, drying, and screening. The CNTs improved upon the polarization efficiency of the PVDF/BTO composite and the  $d_{33}$  value was increased from 0.7 to 2.6 pC/N. The recorded output voltage was 19.3 V, with an output current of 415 nA.



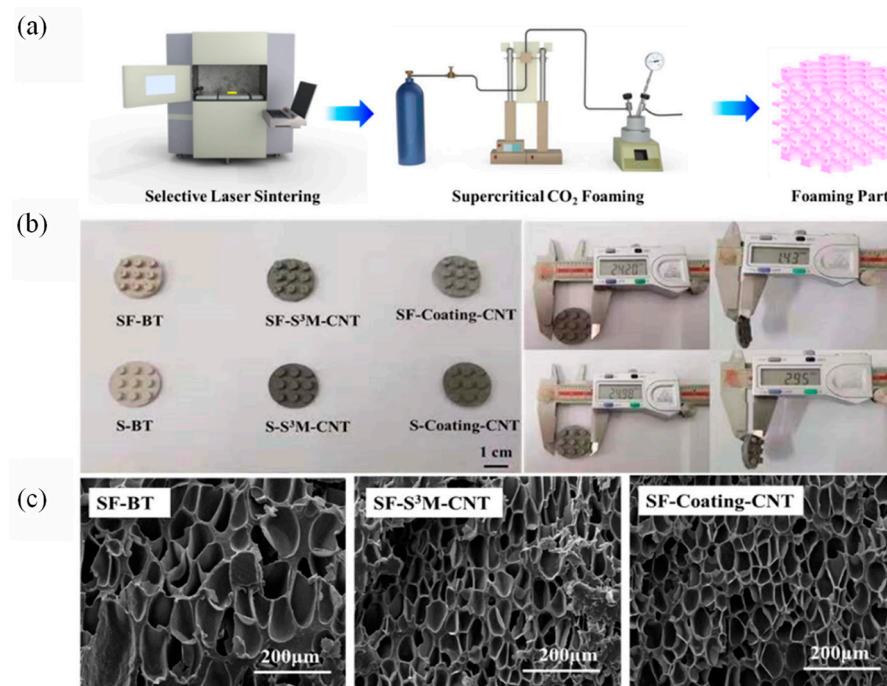


**Figure 8.** (a) Schematic diagram of the preparation of porous foam using Sc-CO<sub>2</sub>. (b) Actual photograph of printed device. (c) SEM image of pore morphology [116]. Reprinted with permission from Qian and Kang. (2021). Copyright © 2021 American Chemical Society.

In the case of DIW, a syringe is filled with the material ink, and appropriate pressure is used to print the material on the substrate. Thus, it is necessary to produce a printing ink with an appropriate viscosity, as the viscosity of the ink strongly affects the fabrication of the device. The ink experiences a shear strain while passing through the needle, which reduces the viscosity of the ink. After the release of the shear strain, the viscosity suddenly increases, which stops the printed ink from spreading. Thus, to produce high-resolution printing, the shear thickness must be maintained [117]. Zhou et al. [118] noted that 3D printing is unsuitable for stretchable devices; it reduces effective contact, which hinders the overall performance of the fabricated device. To overcome this obstacle, they fabricated a PENG using the kirigami technique. They demonstrated the fabrication of a flexible and stretchable PENG, while maintaining the ease of fabrication (Figure 9a). A device based on BTO/P(VDF-TrFE) was fabricated with an Ag flake electrode, and a T-joint-cut kirigami structure was demonstrated (Figure 9). The fabricated device could harvest energy through stretching as well as pressing; the device could withstand being stretched by more than 300% without reducing its output performance. This device produced an open-circuit voltage of 6 V with a short-circuit current of 2  $\mu\text{A}/\text{cm}^2$  (Figure 9b,c), and the maximum power density achieved was 1.4  $\mu\text{W}/\text{cm}^2$ . Another easy printing method used in the fabrication is screen-printing; Li et al. [119] demonstrated the fabrication of a PENG using screen-printing of the surface-modified BTO/PVDF nanocomposite. Surface modification was performed using a triethoxy(octyl)silane (TOs) coating; consequently, the TOs coating prevented the agglomeration of BTO nanoparticles, reduced defects, and improved the output performance. A device with well-dispersed BTO nanoparticles exhibited an output performance of 20 V after 7500 cycles. A power density of 15.6  $\mu\text{W}/\text{cm}^2$  was achieved, which was 150% higher than that of an ordinary BTO/PVDF-based PENG.

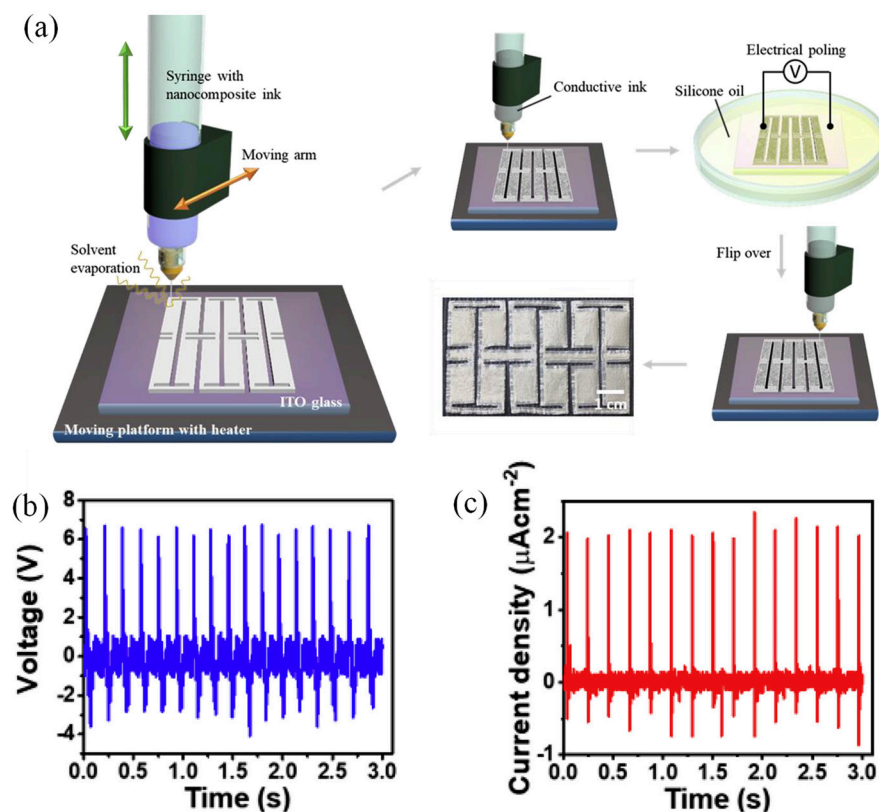


**Figure 9.** Fabrication of a 3D-printed kirigami PENG. (a) Schematic diagram of a 3D-printed PENG with kirigami structure. (b) Output voltage of the fabricated device. (c) Current density with 20 wt% of BaTiO<sub>3</sub> NP/P(VDF-TrFE) at 60 N at 5 Hz on a 1 cm<sup>2</sup> area [118]. Adapted with permission from Zhau (2020). Copyright © 2020 Elsevier.

### 3.7. Hybrid Structures

The coupling of two or more nanogenerators together is referred to as a hybrid structure. Superior performance is a promising feature of hybrid structures, and the output of such structures is the sum of more than one effect, which improves the performance. An HNG is a type of nanogenerator that can harvest energy from various sources. Numerous combinations have been investigated, for example, piezo-tribo and piezo-pyro hybrids. In this system, the same nanogenerator simultaneously exploits triboelectric and piezoelectric effects. The ability to harness energy from different sources simultaneously improves the efficiency of the device. In 2014, Xue et al. [22] reported a novel arc-shaped nanogenerator based on piezoelectric and triboelectric mechanisms. They developed a piezo-tribo-nanogenerator based on BTO/PDMS. The BTO layer acted as the piezo-electric layer in the assembly, which was placed on an ITO/polyethylene terephthalate (PET) insulation layer. The PDMS layer maintained the optimal separation between the top and bottom surfaces. Al foil was utilized as the bottom electrode. The peak-to-peak voltage achieved using this hybrid device was 22 V, with a current density of 1.13  $\mu\text{A}$ .

Han et al. [120] investigated and compared six different piezo-tribo combinations based on the number of terminals connected to the materials. Furthermore, Han et al. compared numerical simulations and experimental measurements of piezo-tribo-nanogenerators in different cases. Their numerical studies led them to conclude that the coupling of piezoelectric and triboelectric effects can be controlled by manipulating the structure, the polarization direction, and the electrode connection. Moreover, the possibility of a zero output due to the negative coupling between the piezoelectric and triboelectric effect could not be ruled out. Next, they concluded that the output could be modulated by realizing the piezoelectric-triboelectric nanogenerator (PE-TENG) in successive and simultaneous coupling modes. The enhancing or weakening mode could be determined based only on

the structure, polarization direction, and electrode connection, regardless of the coupling mode. The output could be modulated in the simultaneous coupling mode by using an appropriate design that allowed the stress inside the piezoelectric material to change with the gap between the two connected surfaces in a specific relationship. This approach has the advantage of achieving the desired output. Furthermore, they concluded that each structure could generate a multilevel electric output using different electrode connections.

In recent years, several approaches have been reported; Mahmud et al. [121] designed an HNG via the integration of organic and inorganic nanostructured materials. They fabricated a device wherein the bottom part operated as a piezoelectric component. The piezoelectric element was fabricated by growing ZnO nanostructures on a chromium-deposited shim substrate using a hydrothermal method. Subsequently, poly(methyl methacrylate) (PMMA) was used to cover the ZnO nanostructure and Al was deposited on it, which formed the piezoelectric part. The triboelectric part consisted of a polytetrafluoroethylene (PTFE) layer, and an Au layer was deposited on it. Reactive ion etching was employed to form nanostructures on the PTFE surface. A copper layer was deposited on the nanostructured PTFE layer to form the electrode. Using double-sided copper tape, an arc-shaped PET was affixed to the PTFE substrate. Finally, both the piezoelectric and triboelectric parts were assembled. The HNG produced 186 V of output voltage, with a current density of  $10.02 \mu\text{A}/\text{cm}^2$ . An average peak power density of  $1.864 \text{ mW}/\text{cm}^2$  was achieved.

In 2020, Patnam et al. [122] utilized Ca-doped BTO to fabricate a piezo-tribo-HNG (Figure 10A(a)), thereby demonstrating a simple fabrication technique. Ca-BTO micro-particles (MPs) were synthesized via a solid-state reaction. Subsequently, the synthesized Ca-BTO MPs were mixed with the PDMS, and the PDMS/Ca-BTO composite film was incorporated as the active material in the assembly (Figure 10A(b)). Next, the developed composite film was laminated on Al tape and glued with a flexible acrylic substrate. Al was employed as a positive triboelectric material, and the top electrode was prepared by attaching a piece of Al to an acrylic substrate. Finally, the top and bottom components were fastened using cellophane tape to form an arc-shaped Ca-BTO-based HNG. The fabricated device exhibited a closed-circuit current and open-circuit voltage of  $34 \mu\text{A}$  and  $550 \text{ V}$ , respectively (Figure 10A(c)), with a maximum power density of  $23.6 \text{ W}/\text{m}^2$ .

Recently, investigations on the synergetic effects of morphology, doping, and hybrid structures have been trending in HNG. For example, Patnam et al. [123] fabricated an HNG device based on Y-doped ZnO nanoflowers. Y-ZnO nanoflowers were synthesized and composited with PDMS using a wet chemical precipitation method. An HNG device was fabricated by attaching the top and bottom components. Both strategies were exploited further to enhance the performance of the HNG. An output voltage and current of  $247 \text{ V}$  and  $7 \mu\text{A}$ , respectively, were achieved.

In addition, several studies on piezo-pyro-HNGs have been reported. Most piezoelectric materials exhibit pyroelectric properties. Yun et al. [124] demonstrated the fabrication of a piezo-tribo hybrid by embedding an MXene-based bifunctional conductive filler, which boosted the performance. As the incorporation of an active material eventually reduces the flexibility of polymer, in that study, the authors added a conductive filler which helped to maintain a low concentration of ceramic filler and a high dielectric constant. They utilized MXene as a conductive filler, BaTiO<sub>3</sub> as an active piezoelectric material, and PDMS as a polymer matrix. The F atoms present in the MXene improved the electrical output generation, which was theoretically and experimentally analyzed. The fabricated device provided an output voltage of  $80 \text{ V}$ , with an output current of  $14 \mu\text{A}$ . The fabricated device was utilized for a human manipulation system and a material detection system. Zhang et al. [125] fabricated a device based on the coupled piezoelectric-triboelectric-pyroelectric effect (Figure 10B(a)). The fabricated device was able to simultaneously harvest mechanical, thermal, and solar energy. The fabricated device exhibited a significant improvement in output performance. The fabricated device consisted of three parts: PZT with piezoelectric, pyroelectric, and photoelectric active material. The polyamide (nylon) acted as a flexible vibrating film to generate a triboelectric effect; additionally, it exerted strain on

the neighboring PZT film. Ag was used to form the bottom electrode, whereas ITO film, combined with Ag nanowire/PDMS attached to the PZT film, acted as the top electrode. A radiator, an adjacent temperature device, acted as the final thermoelectric component. This multi-effect device harvested energy from multiple sources and exhibited the potential to deliver superior performance (Figure 10B(c)).

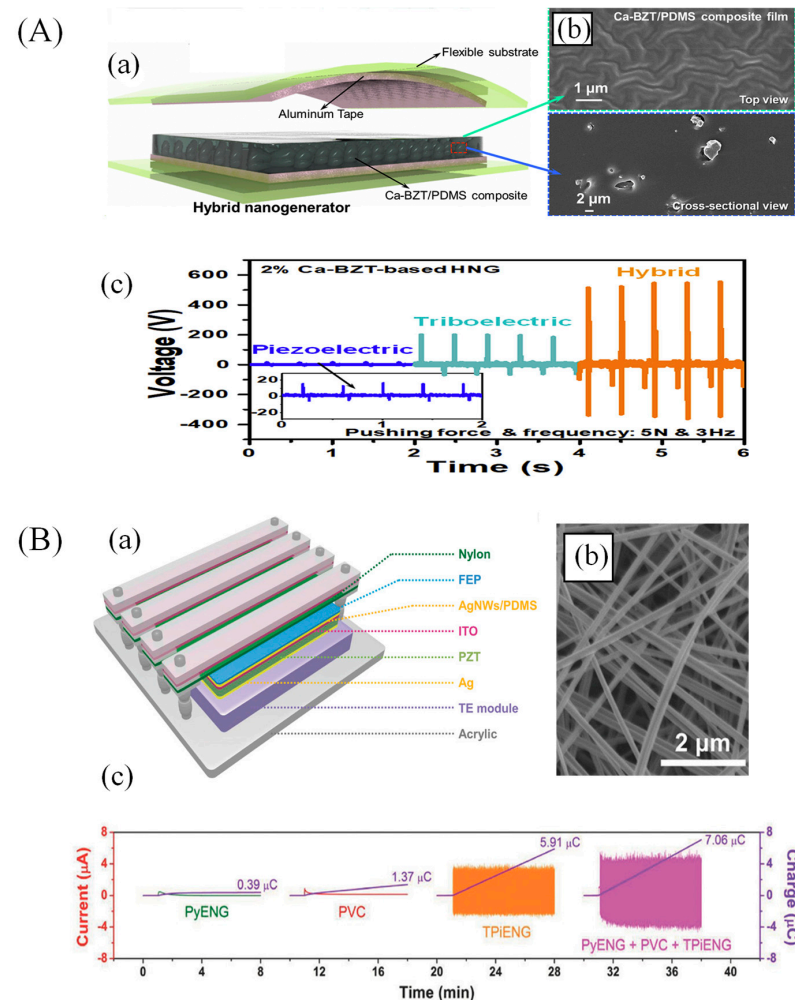


**Figure 10.** (A) A Ca-doped BaTiO<sub>3</sub>-based composite piezo-tribo hybrid nanogenerator. (a) Schematic diagram of BaTiO<sub>3</sub>-based hybrid nanogenerator. (b) Top and cross-sectional FE-SEM view of Ca-BaTiO<sub>3</sub>/PDMS composite film. (c) Comparison of output performance of a fabricated nanogenerator operating in piezoelectric, triboelectric, and hybrid modes [122]. Adapted with permission from Patnam et al. (2020). Copyright © 2020 Elsevier. (B) (a) One structure-based multi-effect (piezo-tribo-pyro-photoelectric effect) hybrid nanogenerator. (b) SEM image of as-prepared AgNWs. (c) Comparative and combined charge transfer of multi-effects [125]. Adapted with permission from Yang et al. (2016) © 2016 WILEY-VCH Verlag GmbH and Co. KGaA, Weinheim.

#### 4. Biomedical Applications

Several state-of-the-art applications of PENGs have been reported in various sectors. The majority of these have been biomedical and health-monitoring applications, owing to their high sensitivity and self-powered nature. As mentioned above, utilizing a battery for a miniaturized device is practically impossible. In this era of the Internet of Things (IoT), self-powered devices play a significant role: they do not require frequent maintenance, and they come with size benefits. In this section, we discuss the different applications of nanogenerators in the biomedical and health-monitoring sectors.

#### 4.1. Health Monitoring

The use of PENGs contributes significantly to self-powered health monitoring devices. The integration of PENGs with health-monitoring sensors can be used to overcome the existing limitations related to powering healthcare devices.

Ravikumar et al. [126] fabricated a PENG based on a metal phenolic coordination framework (MPCF) and a polymer composite. The composite comprised copper oxide nanosphere-tannic acid (CuO-TA) and copper-tannic acid (Cu-TA) nanocube-based MPCF and PVDF. A  $2 \times 2$  cm MPCF composite film was sandwiched between two copper electrodes, and the entire assembly was encapsulated in PDMS to fabricate the device. They compared the output of two different composites (CuO-TA/PVDF and Co-TA/PVDF) and observed a huge difference in performance. The CuO-TA/PVDF and Cu-TA generated output voltages of 40.20 V and 8.90 V, with currents of  $4.40 \mu\text{A}$  and  $3.80 \mu\text{A}$ , respectively. The device was used for the physiological monitoring and harvesting of biological energy. Assuming the condition of increasing heart disease, the authors utilized the CuO-TA/PVDF-based PENG as a physiological monitor and claimed that heart attacks are preventable if symptoms, such as real-time heart rate and arterial pulse [127], can be monitored. To investigate its efficiency and workability, the fabricated device was attached to a 22-year-old healthy person and their heart rate was monitored before and after exercise; the recorded values were approximately 76 and 145 BPM, respectively. The comparison of the results with values measured on a commercially available device suggested that the results were quite accurate. This indicated the sensitivity and applicability of the fabricated device. Furthermore, the authors linked PENG to the IoT to improve its application performance; this allowed the user to access their pulse rate remotely from anywhere. All the fabricated devices were flexible, self-powered, and sufficiently sensitive to distinguish between normal and accelerated pulse rates. This makes PENGs suitable for application in several health monitoring applications. Another attempt was made to develop a wireless self-powered hearth sensor. Rana et al. [128] demonstrated the fabrication of a self-powered, auto-operated wireless sensor based on porous carbon, as shown in Figure 11A(a–c). The fabricated PENG was highly reliable, thus rendering it suitable for different applications, even in inconsistent environments. An output current of  $22 \mu\text{A}$  and a peak-to-peak voltage of 84.5 V were realized; in addition, the fabricated device was environmentally friendly. An entire self-powered network was built for sensing purposes, as shown in Figure 11A(d).

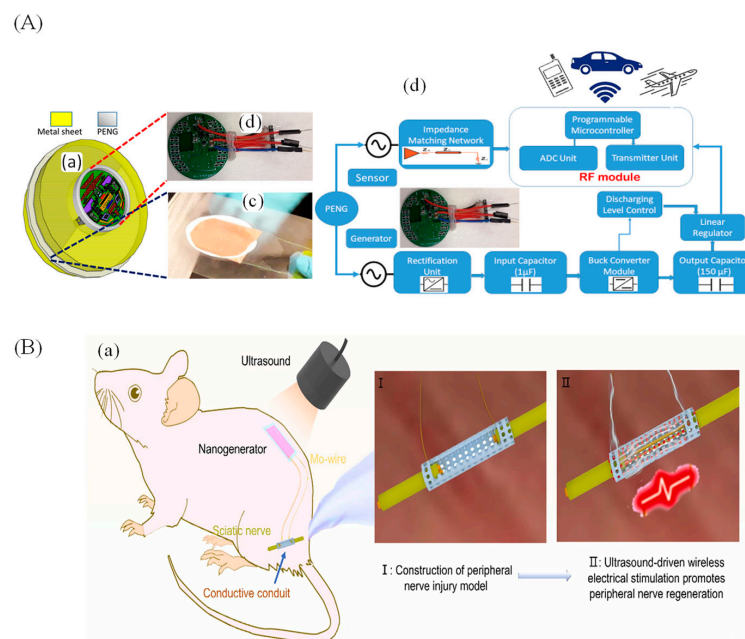


**Figure 11.** (A) Wireless sensor based on a porous PVDF-based PENG. (a) Functional component of the fabricated sensor, which was made up of porous PVDF-PENG and an integrated circuit unit.

(b) Actual image of the fabricated device. (c) Actual image of a fabricated porous PVDF device. (d) Block diagram of the entire sensing system [128]. Adapted with permission from Rana et al. (2020) Copyright © 2020 American Chemical Society (B) Graphical representation of implant in a rat. (a) In vivo electrical simulator in a rat based on a PHBV/PLLA/KNN film nanogenerator with the combined use of ultrasound to enhance peripheral nerve repair [129]. Adapted with permission from Wu et al. (2022). Copyright © 2022 Elsevier.

#### 4.2. Bio Implant

PENGs have also been explored for implantable applications owing to the biodegradable properties of piezoelectric materials. Considering this advantage, Wu et al. [129] developed a PENG to enhance the repair of nerve tissues. They fabricated a device based on KNN, a self-powered in vivo electric stimulator, based on KNN, poly(L-lactic acid) (PLLA), and the proposed Poly(3-hydroxybutyrate-co-3-hydroxyvalerate) (PHBV). Poly(lactic acid) (PLA) or Poly( $\epsilon$ -caprolactone) (PCL) was used for encapsulation, as shown in Figure 11B(a,I,II). The fabricated device was biodegradable and able to harvest energy from ultrasounds. They investigated the functionality of the device in different media, such as water and cell culture, to confirm its biodegradable nature. Furthermore, the fabricated device was implanted in a lab rat (Figure 11B(a)) for 3 weeks. They observed no signs of organ damage in rats and concluded that the fabricated devices were safe for in vitro and in vivo applications. The fabricated device successfully delivered electrical stimuli and promoted nerve repair and monitoring without the use of rectifiers (Figure 11B). Azimi et al. [130] introduced a self-powered cardiac pacemaker based on the polymer PVDF. PVDF is a piezoelectric polymer that is safe and bio-compatible. Batteries have a limited life span, after which they require replacement. We can overcome this limitation with the use of self-powered devices. In the abovementioned study, the author fabricated a PVDF/ZnO/rGO-based PENG using the electrospinning method to power a pacemaker. The pacemaker was tested on an animal model. After the implantation of a self-powered pacemaker on the lateral wall of the left ventricle of a dog animal model, the PENG harvested 0.487  $\mu$ J of energy with every heartbeat. This could represent a great step toward the fabrication of smart implant devices, which shows the future potential of self-powered implant devices. Shrama et al. [131] fabricated an electric stimulator for the acceleration of wound repair. The fabricated device was based on PVDF. They fabricated a piezoelectric hydrogel component made from carbonized polydopamine/polydopamine/polyacrylamide paired with an electrospun PVDF membrane. The hydrogel exhibited good mechanical strength, which supports activities such as walking, stretching, etc. The fabricated film encouraged the growth of cells via electric stimulation produced by body movements; in addition, it provided bacterial protection to the underlying wound.

### 5. Summary and Outlook

PENGs have attracted significant attention owing to the outstanding achievements made in relation to these devices in recent years, and focus is now being placed on the fabrication of high-performance PENGs in energy conversion devices. In addition, regarding flexible and wearable electronics, a focus is being placed on more flexible, reliable, and bio-safe piezoelectric devices based on organic materials and piezoelectric polymers, such as PVDF and P(VDF-TrFE). Thus, PENGs must provide a high output voltage and current with a long and uninterrupted operating life, which can be achieved by customizing piezoelectric materials using strategies such as morphological tuning, doping, developing composites, and synthesis techniques. The overall growth of high-performance PENGs was catalyzed by newly introduced approaches such as 3D printing and fabrication, as well as different device strategies such as an electrode, surface, and interfacial modifications. Novel materials, such as g-C<sub>3</sub>N<sub>4</sub> and BNN, which have superior piezoelectric properties compared with previously reported materials, are also being explored. A new feature of nanogenerators is HNG, which harvests energy from multiple sources simultaneously, and such a hybrid structure drastically improves the output performance.

Overall, the future applications of PENGs are based on the following aspects. (1) PENGs have been recognized as potential candidates for biomedical applications. A PENG can be used as a power source for microdevices or as a self-powered bio-implant. The growth of recent bio-implants has slowed due to the limitations of their power sources. Batteries have major drawbacks, such as the use of bio-hazard materials and their high fabrication and maintenance costs. By contrast, PENGs can be bio-safe, involve low-cost fabrication processes, and do not require frequent maintenance. They are smaller than existing batteries and are thus perfect candidates for biomedical applications. (2) To catalyze the growth of PENGs, finding new approaches in order to improve their existing performance is a necessary step. The output performance of the device can be improved by combining different strategies during fabrication. Specific strategies can be exploited; for example, Liu et al. [113] combined doping and interfacial modification. (3) New materials, such as g-C<sub>3</sub>N<sub>4</sub> and BNN, exhibit a high piezoelectric response compared to existing piezoelectric materials because of their highly crystalline nature. These materials can be synthesized using simple methods, such as solid-state reactions. (4) The fabrication of hybrid structures is a potential approach to improving performance. Hybrid-structure nanogenerators can harvest multiple energy sources simultaneously, which results in considerable improvements in the output voltage and current.

**Author Contributions:** Writing—original draft preparation and curation, O.Y.P. Review and editing, O.Y.P., S.B.P., S.L.P. and R.S.R. reviewed the article. Supervision N.L.T., S.B.P. and S.L. All authors have read and agreed to the published version of the manuscript.

**Funding:** This work was supported by a National Research Foundation of Korea (NRF) grant funded by the Korean government (2021R1A2C1011248).

**Acknowledgments:** NLT is thankful to DST-SERB for providing the financial assistance through Teachers Associateship for Research Excellence (TARE) scheme (TAR/2021/000307). The financial assistance through DST-PURSE Phase-II (2018–2023) and UGC-DSA Phase-II (2018–2023) is highly acknowledged. SBP is thankful to Council of Scientific and Industrial Research for providing CSIR-SRA fellowship (Pool no. 9081-A) under Pool scheme.

**Conflicts of Interest:** The authors declare that they have no known competing financial interests.

## References

1. Weber, M.J.; Yoshihara, Y.; Sawaby, A.; Charthad, J.; Chang, T.C.; Arbabian, A. A Miniaturized Single-Transducer Implantable Pressure Sensor with Time-Multiplexed Ultrasonic Data and Power Links. *IEEE J. Solid-State Circuits* **2018**, *53*, 1089–1101. [[CrossRef](#)]
2. Hulsmans, M.; Aguirre, A.D.; Bonner, M.D.; Bapat, A.; Cremer, S.; Iwamoto, Y.; King, K.R.; Swirski, F.K.; Milan, D.J.; Weissleder, R.; et al. A Miniaturized, Programmable Pacemaker for Long-Term Studies in the Mouse. *Circ. Res.* **2018**, *123*, 1208–1219. [[CrossRef](#)] [[PubMed](#)]
3. Khan, W.; Jia, Y.; Madi, F.; Weber, A.; Ghovanloo, M.; Li, W. *A Miniaturized, Wirelessly-Powered, Reflector-Coupled Single Channel Opto Neurostimulator*; IEEE: Belfast, UK, 2018; p. 174.
4. Glynne-Jones, P.; White, N.M. Self-powered systems: A review of energy sources. In *Sensor Review*; Emerald Group Publishing Ltd.: Bingley, UK, 2001; pp. 91–97.
5. Hsu, C.L.; Su, I.L.; Hsueh, T.J. Sulfur-Doped-ZnO-Nanospire-Based Transparent Flexible Nanogenerator Self-Powered by Environmental Vibration. *RSC Adv.* **2015**, *5*, 34019–34026. [[CrossRef](#)]
6. Jung, J.H.; Lee, M.; Hong, J.-I.; Ding, Y.; Chen, C.Y.; Chou, L.J.; Wang, Z.L. Lead-Free NaNbO<sub>3</sub> Nanowires for a High Output Piezoelectric Nanogenerator. *ACS Nano* **2011**, *5*, 10041–10046. [[CrossRef](#)]
7. Wu, C.; Wang, A.C.; Ding, W.; Guo, H.; Wang, Z.L. Triboelectric Nanogenerator: A Foundation of the Energy for the New Era. *Adv. Energy Mater.* **2019**, *9*, 1802906. [[CrossRef](#)]
8. Xue, H.; Yang, Q.; Wang, D.; Luo, W.; Wang, W.; Lin, M.; Liang, D.; Luo, Q. A Wearable Pyroelectric Nanogenerator and Self-Powered Breathing Sensor. *Nano Energy* **2017**, *38*, 147–154. [[CrossRef](#)]
9. Gao, Z.; Zhou, J.; Gu, Y.; Fei, P.; Hao, Y.; Bao, G.; Wang, Z.L. Effects of Piezoelectric Potential on the Transport Characteristics of Metal-ZnO Nanowire-Metal Field Effect Transistor. *J. Appl. Phys.* **2009**, *105*, 113707. [[CrossRef](#)]
10. Mason, W.P. Piezoelectricity, Its History and Applications. *J. Acoust. Soc. Am.* **1980**, *68*, S39. [[CrossRef](#)]
11. Wang, Z.L.; Song, J. Piezoelectric Nanogenerators Based on Zinc Oxide Nanowire Arrays. *Science* **2006**, *312*, 242–246. [[CrossRef](#)]
12. Price, A.S.; Savchenko, A.K.; Narozhny, B.N.; Allison, G.; Ritchie, D.A. Giant Fluctuations of Coulomb Drag in a Bilayer System. *Science* **2007**, *316*, 99–102. [[CrossRef](#)]

13. Yang, R.; Qin, Y.; Dai, L.; Wang, Z.L. Power Generation with Laterally Packaged Piezoelectric Fine Wires. *Nat. Nanotechnol.* **2009**, *4*, 34–39. [[CrossRef](#)] [[PubMed](#)]
14. Zhu, G.; Yang, R.; Wang, S.; Wang, Z.L. Flexible High-Output Nanogenerator Based on Lateral ZnO Nanowire Array. *Nano Lett.* **2010**, *10*, 3151–3155. [[CrossRef](#)] [[PubMed](#)]
15. Momeni, K.; Odegard, G.M.; Yassar, R.S. Nanocomposite Electrical Generator Based on Piezoelectric Zinc Oxide Nanowires. *J. Appl. Phys.* **2010**, *108*, 114303. [[CrossRef](#)]
16. Maria Joseph Raj, N.P.; Ks, A.; Khandelwal, G.; Alluri, N.R.; Kim, S.J. A Lead-Free Ferroelectric Bi<sub>0.5</sub>Na<sub>0.5</sub>TiO<sub>3</sub> based Flexible, Lightweight Nanogenerator for Motion Monitoring Applications. *Sustain. Energy Fuels* **2020**, *4*, 5636–5644. [[CrossRef](#)]
17. Wang, R.C.; Lin, Y.C.; Chen, H.C.; Lin, W.Y. Energy Harvesting from G-C<sub>3</sub>N<sub>4</sub> Piezoelectric Nanogenerators. *Nano Energy* **2021**, *83*, 105743. [[CrossRef](#)]
18. Kim, K.H.; Kumar, B.; Lee, K.Y.; Park, H.K.; Lee, J.H.; Lee, H.H.; Jun, H.; Lee, D.; Kim, S.W. Piezoelectric Two-Dimensional Nanosheets/Anionic Layer Heterojunction for Efficient Direct Current Power Generation. *Sci. Rep.* **2013**, *3*, 2017. [[CrossRef](#)]
19. Verma, K.; Bharti, D.K.; Badatya, S.; Srivastava, A.K.; Gupta, M.K. A High Performance Flexible Two Dimensional Vertically Aligned ZnO Nanodisc Based Piezoelectric Nanogenerator via surface Passivation. *Nanoscale Adv.* **2020**, *2*, 2044–2051. [[CrossRef](#)]
20. Gu, L.; Liu, J.; Cui, N.; Xu, Q.; Du, T.; Zhang, L.; Wang, Z.; Long, C.; Qin, Y. Enhancing the Current Density of a Piezoelectric Nanogenerator Using a Three-Dimensional Intercalation Electrode. *Nat. Commun.* **2020**, *11*, 1030. [[CrossRef](#)]
21. Song, S.; Li, Y.; Wang, Q.; Zhang, C. Boosting Piezoelectric Performance with a New Selective Laser Sintering 3D Printable PVDF/Graphene Nanocomposite. *Compos. Part A Appl. Sci. Manuf.* **2021**, *147*, 106452. [[CrossRef](#)]
22. Xue, C.; Li, J.; Zhang, Q.; Zhang, Z.; Hai, Z.; Gao, L.; Feng, R.; Tang, J.; Liu, J.; Zhang, W.; et al. A Novel Arch-Shape Nanogenerator Based on Piezoelectric and Triboelectric Mechanism for Mechanical Energy Harvesting. *Nanomaterials* **2014**, *5*, 36–46. [[CrossRef](#)]
23. Fan, F.R.; Tang, W.; Wang, Z.L. Flexible Nanogenerators for Energy Harvesting and Self-Powered Electronics. *Adv. Mater.* **2016**, *28*, 4283–4305. [[CrossRef](#)]
24. Xu, S.; Qin, Y.; Xu, C.; Wei, Y.; Yang, R.; Wang, Z.L. Self-Powered Nanowire Devices. *Nat. Nanotechnol.* **2010**, *5*, 366–373. [[CrossRef](#)]
25. Niu, X.; Jia, W.; Qian, S.; Zhu, J.; Zhang, J.; Hou, X.; Mu, J.; Geng, W.; Cho, J.; He, J.; et al. High-Performance PZT-Based Stretchable Piezoelectric Nanogenerator. *ACS Sustain. Chem. Eng.* **2019**, *7*, 979–985. [[CrossRef](#)]
26. Wu, W.; Bai, S.; Yuan, M.; Qin, Y.; Wang, Z.L.; Jing, T. Lead Zirconate Titanate Nanowire Textile Nanogenerator for Wearable Energy-Harvesting and Self-Powered Devices. *ACS Nano* **2012**, *6*, 6231–6235. [[CrossRef](#)] [[PubMed](#)]
27. Budimir, M.; Damjanovic, D.; Setter, N. Piezoelectric Anisotropy-Phase Transition Relations in Perovskite Single Crystals. *J. Appl. Phys.* **2003**, *94*, 6753–6761. [[CrossRef](#)]
28. Lee, W.H.; Su, C.Y. Improvement in the Temperature Stability of a BaTiO<sub>3</sub>-Based Multilayer Ceramic Capacitor by Constrained Sintering. *J. Am. Ceram. Soc.* **2007**, *90*, 3345–3348. [[CrossRef](#)]
29. Li, Y.; Liao, Z.; Fang, F.; Wang, X.; Li, L.; Zhu, J. Significant Increase of Curie Temperature in Nano-Scale BaTiO<sub>3</sub>. *Appl. Phys. Lett.* **2014**, *105*, 182901. [[CrossRef](#)]
30. Zhang, Y.; Sun, H.; Chen, W. Influence of Cobalt and Sintering Temperature on Structure and Electrical Properties of BaZr<sub>0.05</sub>Ti<sub>0.95</sub>O<sub>3</sub> Ceramics. *Ceram. Int.* **2015**, *41*, 8520–8532. [[CrossRef](#)]
31. Acosta, M.; Novak, N.; Rojas, V.; Patel, S.; Vaish, R.; Koruza, J.; Rossetti, G.A.; Rödel, J. BaTiO<sub>3</sub>-based piezoelectrics: Fundamentals, current status, and perspectives. In *Applied Physics Reviews*; American Institute of Physics Inc.: College Park, MD, USA, 2017.
32. Liu, W.; Ren, X. Large Piezoelectric Effect in Pb-Free Ceramics. *Phys. Rev. Lett.* **2009**, *103*, 257602. [[CrossRef](#)]
33. Zhou, Z.; Bowland, C.C.; Malakooti, M.H.; Tang, H.; Sodano, H.A. Lead-Free 0.5Ba(Zr<sub>0.2</sub>Ti<sub>0.8</sub>)O<sub>3</sub>-0.5(Ba<sub>0.7</sub>Ca<sub>0.3</sub>)TiO<sub>3</sub> Nanowires for Energy Harvesting. *Nanoscale* **2016**, *8*, 5098–5105. [[CrossRef](#)]
34. Caruntu, D.; Rostamzadeh, T.; Costanzo, T.; Saleemizadeh Parizi, S.; Caruntu, G. Solvothermal Synthesis and Controlled Self-Assembly of Monodisperse Titanium-Based Perovskite Colloidal Nanocrystals. *Nanoscale* **2015**, *7*, 12955–12969. [[CrossRef](#)] [[PubMed](#)]
35. Xue, P.; Wu, H.; Xia, W.; Pei, Z.; Lu, Y.; Zhu, X. Molten Salt Synthesis of BaTiO<sub>3</sub> Nanorods: Dielectric, Optical Properties, and Structural Characterizations. *J. Am. Ceram. Soc.* **2019**, *102*, 2325–2336. [[CrossRef](#)]
36. Philippot, G.; Elissalde, C.; Maglione, M.; Aymonier, C. Supercritical fluid technology: A reliable process for high quality BaTiO<sub>3</sub> based nanomaterials. In *Advanced Powder Technology*; Elsevier B.V.: Amsterdam, The Netherlands, 2014; pp. 1415–1429.
37. Zhao, Z.; Buscaglia, V.; Viviani, M.; Buscaglia, M.T.; Mitoseriu, L.; Testino, A.; Nygren, M.; Johnsson, M.; Nanni, P. Grain-Size Effects on the Ferroelectric Behavior of Dense Nanocrystalline BaTiO<sub>3</sub> Ceramics. *Phys. Rev. B Condens. Matter. Mater. Phys.* **2004**, *70*, 024107. [[CrossRef](#)]
38. Wang, G.; Li, Y.; Murray, C.A.; Tang, C.C.; Hall, D.A. Thermally-Induced Phase Transformations in Na<sub>0.5</sub>Bi<sub>0.5</sub>TiO<sub>3</sub>-KNbO<sub>3</sub> Ceramics. *J. Am. Ceram. Soc.* **2017**, *100*, 3293–3304. [[CrossRef](#)]
39. Hong, C.H.; Fan, Z.; Tan, X.; Kang, W.S.; Ahn, C.W.; Shin, Y.; Jo, W. Role of Sodium Deficiency on the Relaxor Properties of Bi<sub>1/2</sub>Na<sub>1/2</sub>TiO<sub>3</sub>-BaTiO<sub>3</sub>. *J. Eur. Ceram. Soc.* **2018**, *38*, 5375–5381. [[CrossRef](#)]
40. Ren, X.; Fan, H.; Zhao, Y.; Liu, Z. Flexible Lead-Free BiFeO<sub>3</sub>/PDMS-Based Nanogenerator as Piezoelectric Energy Harvester. *ACS Appl. Mater. Interfaces* **2016**, *8*, 26190–26197. [[CrossRef](#)]
41. Park, T.J.; Mao, Y.; Wong, S.S. Synthesis and Characterization of Multiferroic BiFeO<sub>3</sub> Nanotubes. *Chem. Commun.* **2004**, *23*, 2708–2709. [[CrossRef](#)]



42. Kadomtseva, A.M.; Popov, Y.F.; Pyatakov, A.P.; Vorob'Ev, G.P.; Zvezdin, A.K.; Viehland, D. Phase Transitions in Multiferroic BiFeO<sub>3</sub> Crystals, Thin-Layers, and Ceramics: Enduring Potential for a Single Phase, Room-Temperature Magnetoelectric "Holy Grail". *Phase Transit.* **2006**, *79*, 1019–1042. [[CrossRef](#)]
43. Bennett, J.; Bell, A.J.; Stevenson, T.J.; Comyn, T.P. Tailoring the Structure and Piezoelectric Properties of BiFeO<sub>3</sub>-(K<sub>0.5</sub>Bi<sub>0.5</sub>)TiO<sub>3</sub>-PbTiO<sub>3</sub> Ceramics for High Temperature Applications. *Appl. Phys. Lett.* **2013**, *103*, 152901. [[CrossRef](#)]
44. Sando, D.; Barthélémy, A.; Bibes, M. BiFeO<sub>3</sub> epitaxial thin films and devices: Past, present and future. In *Journal of Physics Condensed Matter*; Institute of Physics Publishing: Bristol, UK, 2014.
45. Pan, H.; Li, F.; Liu, Y.; Zhang, Q.; Wang, M.; Lan, S.; Zheng, Y.; Ma, J.; Gu, L.; Shen, Y.; et al. Ultrahigh-Energy Density Lead-Free Dielectric Films via Polymorphic Nanodomain Design Downloaded from. *Science* **2019**, *365*, 578–582. [[CrossRef](#)]
46. Deng, Y.; Wang, J.; Zhang, C.; Ma, H.; Bai, C.; Liu, D.; Wu, F.; Yang, B. Structural and Electric Properties of MnO<sub>2</sub>-Doped KNN-LT Lead-Free Piezoelectric Ceramics. *Crystals* **2020**, *10*, 705. [[CrossRef](#)]
47. Swain, S.; Kumar, P.; Agrawal, D.K.; Sonia. Dielectric and Ferroelectric Study of KNN Modified NBT Ceramics Synthesized by Microwave Processing Technique. *Ceram. Int.* **2013**, *39*, 3205–3210. [[CrossRef](#)]
48. Kwak, J.; Kingon, A.I.; Kim, S.H. Lead-Free (Na<sub>0.5</sub>K<sub>0.5</sub>)NbO<sub>3</sub> Thin Films for the Implantable Piezoelectric Medical Sensor Applications. *Mater. Lett.* **2012**, *82*, 130–132. [[CrossRef](#)]
49. Wu, J.; Xiao, D.; Zhu, J. Potassium-sodium niobate lead-free piezoelectric materials: Past, present, and future of phase boundaries. In *Chemical Reviews*; American Chemical Society: Washington, DC, USA, 2015; pp. 2559–2595.
50. Khorrami, G.H.; Kompany, A.; Khorsand Zak, A. Structural and Optical Properties of (K,Na)NbO<sub>3</sub> Nanoparticles Synthesized by a Modified Sol-Gel Method Using Starch Media. *Adv. Powder Technol.* **2015**, *26*, 113–118. [[CrossRef](#)]
51. Zhou, D.; Gu, H.; Hu, Y.; Tian, H.; Wang, Z.; Qian, Z.; Wang, Y. Synthesis, Characterization and Ferroelectric Properties of Lead-Free K<sub>0.5</sub>Na<sub>0.5</sub>NbO<sub>3</sub> Nanotube Arrays. *J. Appl. Phys.* **2011**, *109*, 11410. [[CrossRef](#)]
52. Ghasemian, M.B.; Rawal, A.; Shahrababaki, Z.; Zhang, Q.; Lu, T.; Liu, Y.; Wang, D. Evidence of Phase Coexistence in Hydrothermally Synthesized K<sub>0.5</sub>Na<sub>0.5</sub>NbO<sub>3</sub> nanofibers. *J. Mater. Chem. A Mater.* **2020**, *8*, 8731–8739. [[CrossRef](#)]
53. Brown, L.F.; Carlson, R.L.; Semprntt, J.M. *Spin-Cast P(VDF-TrFE) Films for High Performance Medical Ultrasound Transducers*; IEEE: Belfast, UK, 2006.
54. Jung, I.; Shin, Y.H.; Kim, S.; Choi, J.Y.; Kang, C.Y. Flexible Piezoelectric Polymer-Based Energy Harvesting System for Roadway Applications. *Appl. Energy* **2017**, *197*, 222–229. [[CrossRef](#)]
55. Ye, L.; Chen, L.; Yu, J.; Tu, S.; Yan, B.; Zhao, Y.; Bai, X.; Gu, Y.; Chen, S. High-Performance Piezoelectric Nanogenerator Based on Electrospun ZnO Nanorods/P(VDF-TrFE) Composite Membranes for Energy Harvesting Application. *J. Mater. Sci. Mater. Electron.* **2021**, *32*, 3966–3978. [[CrossRef](#)]
56. Sappati, K.K.; Bhadra, S. Piezoelectric Polymer and Paper Substrates: A Review. *Sensors* **2018**, *18*, 3605. [[CrossRef](#)]
57. Sharma, M.; Srinivas, V.; Madras, G.; Bose, S. Outstanding Dielectric Constant and Piezoelectric Coefficient in Electrospun Nanofiber Mats of PVDF Containing Silver Decorated Multiwall Carbon Nanotubes: Assessing through Piezoresponse Force Microscopy. *RSC Adv.* **2016**, *6*, 6251–6258. [[CrossRef](#)]
58. Sarangi, M.; Bhattacharyya, S.; Behera, R.C. Effect of Temperature on Morphology and Phase Transformations of Nano-Crystalline Silica Obtained from Rice Husk. *Phase Transit.* **2009**, *82*, 377–386. [[CrossRef](#)]
59. Pileni, M.P.; Hammouda, A.; Lisiecki, I.; Motte, L.; Moumen, N.; Tanori, J. Control of the size and shape of nanoparticles. In *Fine Particles Science and Technology*; Springer: Cham, Switzerland, 1996.
60. Singh, O.; Singh, M.P.; Kohli, N.; Singh, R.C. Effect of PH on the Morphology and Gas Sensing Properties of ZnO Nanostructures. *Sens. Actuators B Chem.* **2012**, *166–167*, 438–443. [[CrossRef](#)]
61. Pascariu, P.; Homocianu, M. ZnO-based ceramic nanofibers: Preparation, properties and applications. In *Ceramics International*; Elsevier Ltd.: Amsterdam, The Netherlands, 2019; pp. 11158–11173.
62. Khan, A.; Ali Abbasi, M.; Hussain, M.; Hussain Ibupoto, Z.; Wissting, J.; Nur, O.; Willander, M. Piezoelectric Nanogenerator Based on Zinc Oxide Nanorods Grown on Textile Cotton Fabric. *Appl. Phys. Lett.* **2012**, *101*, 193506. [[CrossRef](#)]
63. Van Ngoc, H.; Kang, D.J. Flexible, Transparent and Exceptionally High Power Output Nanogenerators Based on Ultrathin ZnO Nanoflakes. *Nanoscale* **2016**, *8*, 5059–5066. [[CrossRef](#)]
64. Zhao, Q.L.; He, G.P.; Di, J.J.; Song, W.L.; Hou, Z.L.; Tan, P.P.; Wang, D.W.; Cao, M.S. Flexible Semitransparent Energy Harvester with High Pressure Sensitivity and Power Density Based on Laterally Aligned PZT Single-Crystal Nanowires. *ACS Appl. Mater. Interfaces* **2017**, *9*, 24696–24703. [[CrossRef](#)] [[PubMed](#)]
65. Jin, W.; Wang, Z.; Huang, H.; Hu, X.; He, Y.; Li, M.; Li, L.; Gao, Y.; Hu, Y.; Gu, H. High-Performance Piezoelectric Energy Harvesting of Vertically Aligned Pb(Zr,Ti)O<sub>3</sub> Nanorod Arrays. *RSC Adv.* **2018**, *8*, 7422–7427. [[CrossRef](#)] [[PubMed](#)]
66. Qi, Y.; Jafferis, N.T.; Lyons, K.; Lee, C.M.; Ahmad, H.; McAlpine, M.C. Piezoelectric Ribbons Printed onto Rubber for Flexible Energy Conversion. *Nano Lett.* **2010**, *10*, 524–525. [[CrossRef](#)] [[PubMed](#)]
67. Park, K.-I.; Son, J.H.; Hwang, G.T.; Jeong, C.K.; Ryu, J.; Koo, M.; Choi, I.; Lee, S.H.; Byun, M.; Wang, Z.L.; et al. Highly-Efficient, Flexible Piezoelectric PZT Thin Film Nanogenerator on Plastic Substrates. *Adv. Mater.* **2014**, *26*, 2514–2520. [[CrossRef](#)] [[PubMed](#)]
68. Zhang, X.; Chen, J.; Wang, Y. Hierarchical PbZr<sub>x</sub>Ti<sub>1-x</sub>O<sub>3</sub> Nanowires for Vibrational Energy Harvesting. *ACS Appl. Nano Mater.* **2018**, *1*, 1461–1466. [[CrossRef](#)]
69. Huango, K.C.; Huango, T.C.; Hsieh, W.F. Morphology-Controlled Synthesis of Barium Titanate Nanostructures. *Inorg. Chem.* **2009**, *48*, 9180–9184. [[CrossRef](#)]

70. Lin, Z.H.; Yang, Y.; Wu, J.M.; Liu, Y.; Zhang, F.; Wang, Z.L. BaTiO<sub>3</sub> Nanotubes-Based Flexible and Transparent Nanogenerators. *J. Phys. Chem. Lett.* **2012**, *3*, 3599–3604. [[CrossRef](#)] [[PubMed](#)]
71. Park, K.-I.; Bae, S.B.; Yang, S.H.; Lee, H.I.; Lee, K.; Lee, S.J. Lead-Free BaTiO<sub>3</sub> Nanowires-Based Flexible Nanocomposite Generator. *Nanoscale* **2014**, *6*, 8962–8968. [[CrossRef](#)] [[PubMed](#)]
72. Chen, X.; Li, X.; Shao, J.; An, N.; Tian, H.; Wang, C.; Han, T.; Wang, L.; Lu, B. High-Performance Piezoelectric Nanogenerators with Imprinted P(VDF-TrFE)/BaTiO<sub>3</sub> Nanocomposite Micropillars for Self-Powered Flexible Sensors. *Small* **2017**, *13*, 1604245. [[CrossRef](#)]
73. Sriphan, S.; Nawani, C.; Vittayakorn, N. Influence of Dispersed Phase Morphology on Electrical and Fatigue Properties of BaTiO<sub>3</sub>/PDMS Nanogenerator. *Ceram. Int.* **2018**, *44*, S38–S42. [[CrossRef](#)]
74. Bairagi, S.; Ali, S.W. Investigating the Role of Carbon Nanotubes (CNTs) in the Piezoelectric Performance of a PVDF/KNN-Based Electrospun Nanogenerator. *Soft Matter* **2020**, *16*, 4876–4886. [[CrossRef](#)] [[PubMed](#)]
75. Bairagi, S.; Ali, S.W. Influence of High Aspect Ratio Lead-Free Piezoelectric Fillers in Designing Flexible Fibrous Nanogenerators: Demonstration of Significant High Output Voltage. *Energy Technol.* **2019**, *7*, 1900538. [[CrossRef](#)]
76. Zhang, Y.; Liu, C.; Liu, J.; Xiong, J.; Liu, J.; Zhang, K.; Liu, Y.; Peng, M.; Yu, A.; Zhang, A.; et al. Lattice Strain Induced Remarkable Enhancement in Piezoelectric Performance of ZnO-Based Flexible Nanogenerators. *ACS Appl. Mater. Interfaces* **2016**, *8*, 1381–1387. [[CrossRef](#)] [[PubMed](#)]
77. Wang, X.B.; Song, C.; Li, D.M.; Geng, K.W.; Zeng, F.; Pan, F. The Influence of Different Doping Elements on Microstructure, Piezoelectric Coefficient and Resistivity of Sputtered ZnO Film. *Appl. Surf. Sci.* **2006**, *253*, 1639–1643. [[CrossRef](#)]
78. Sinha, N.; Ray, G.; Bhandari, S.; Godara, S.; Kumar, B. Synthesis and Enhanced Properties of Cerium Doped ZnO Nanorods. *Ceram. Int.* **2014**, *40 Pt A*, 12337–12342. [[CrossRef](#)]
79. Yadav, H.; Sinha, N.; Goel, S.; Kumar, B. Eu-Doped ZnO Nanoparticles for Dielectric, Ferroelectric and Piezoelectric Applications. *J. Alloys Compd.* **2016**, *689*, 333–341. [[CrossRef](#)]
80. Goel, S.; Sinha, N.; Yadav, H.; Godara, S.; Joseph, A.J.; Kumar, B. Ferroelectric Gd-Doped ZnO Nanostructures: Enhanced Dielectric, Ferroelectric and Piezoelectric Properties. *Mater. Chem. Phys.* **2017**, *202*, 56–64. [[CrossRef](#)]
81. Chen, Y.J.; Brahma, S.; Liu, C.P.; Huang, J.L. Enhancement of the Piezoelectric Coefficient in Hexagonal Mg<sub>x</sub>Zn<sub>1-x</sub>O Films at Lower Mg Compositions. *J. Alloys Compd.* **2017**, *728*, 1248–1253. [[CrossRef](#)]
82. Pan, F.; Luo, J.; Yang, Y.; Wang, X.; Zeng, F. Giant Piezoresponse and Promising Application of Environmental Friendly Small-Ion-Doped ZnO. *Sci. China Technol. Sci.* **2012**, *55*, 421–436. [[CrossRef](#)]
83. Goel, S.; Sinha, N.; Yadav, H.; Joseph, A.J.; Kumar, B. Experimental Investigation on the Structural, Dielectric, Ferroelectric and Piezoelectric Properties of La Doped ZnO Nanoparticles and Their Application in Dye-Sensitized Solar Cells. *Phys. E Low Dimens Syst. Nanostruct* **2017**, *91*, 72–81. [[CrossRef](#)]
84. Yang, Y.C.; Song, C.; Wang, X.H.; Zeng, F.; Pan, F. Cr-Substitution-Induced Ferroelectric and Improved Piezoelectric Properties of Zn<sub>1-x</sub>Cr<sub>x</sub>O Films. *J. Appl. Phys.* **2008**, *103*, 074107. [[CrossRef](#)]
85. Yang, Y.C.; Song, C.; Wang, X.H.; Zeng, F.; Pan, F. Giant Piezoelectric D33 Coefficient in Ferroelectric Vanadium Doped ZnO Films. *Appl. Phys. Lett.* **2008**, *92*, 012907. [[CrossRef](#)]
86. Sinha, N.; Goel, S.; Joseph, A.J.; Yadav, H.; Batra, K.; Gupta, M.K.; Kumar, B. Y-Doped ZnO Nanosheets: Gigantic Piezoelectric Response for an Ultra-Sensitive Flexible Piezoelectric Nanogenerator. *Ceram. Int.* **2018**, *44*, 8582–8590. [[CrossRef](#)]
87. Manikandan, M.; Rajagopalan, P.; Patra, N.; Jayachandran, S.; Muralidharan, M.; Mani Prabu, S.S.; Palani, I.A.; Singh, V. Development of Sn-Doped ZnO Based Ecofriendly Piezoelectric Nanogenerator for Energy Harvesting Application. *Nanotechnology* **2020**, *31*, 185401. [[CrossRef](#)]
88. Batra, K.; Sinha, N.; Kumar, B. Tb-Doped ZnO:PDMS Based Flexible Nanogenerator with Enhanced Piezoelectric Output Performance by Optimizing Nanofiller Concentration. *Ceram. Int.* **2020**, *46*, 24120–24128. [[CrossRef](#)]
89. Lee, S.; Lee, J.; Ko, W.; Cha, S.; Sohn, J.; Kim, J.; Park, J.; Park, Y.; Hong, J. Solution-Processed Ag-Doped ZnO Nanowires Grown on Flexible Polyester for Nanogenerator Applications. *Nanoscale* **2013**, *5*, 9609–9614. [[CrossRef](#)]
90. Rafique, S.; Kasi, A.K.; Aminullah; Kasi, J.K.; Bokhari, M.; Shakoor, Z. Fabrication of Br Doped ZnO Nanosheets Piezoelectric Nanogenerator for Pressure and Position Sensing Applications. *Curr. Appl. Phys.* **2021**, *21*, 72–79. [[CrossRef](#)]
91. Alnajjar, M.H.; Sinha, N.; Kumar, B. Remarkably Enhanced Piezoelectric and Ferroelectric Characteristics of Er:ZnO upon Graphene Addition for Wearable Self-Powered Piezoelectric Sensors. *Mater. Res. Bull.* **2023**, *161*, 112149. [[CrossRef](#)]
92. Rehrig, P.W.; Park, S.E.; Trolier-McKinstry, S.; Messing, G.L.; Jones, B.; Shrout, T.R. Piezoelectric Properties of Zirconium-Doped Barium Titanate Single Crystals Grown by Templated Grain Growth. *J. Appl. Phys.* **1999**, *86*, 1657–1661. [[CrossRef](#)]
93. Upadhyay, S.K.; Reddy, V.R.; Bag, P.; Rawat, R.; Gupta, S.M.; Gupta, A. Electro-Caloric Effect in Lead-Free Sn Doped BaTiO<sub>3</sub> ceramics at Room Temperature and Low Applied Fields. *Appl. Phys. Lett.* **2014**, *105*, 112907. [[CrossRef](#)]
94. Alluri, N.R.; Saravanakumar, B.; Kim, S.J. Flexible, Hybrid Piezoelectric Film (BaTi<sub>(1-x)</sub>Zr<sub>x</sub>O<sub>3</sub>)/PVDF Nanogenerator as a Self-Powered Fluid Velocity Sensor. *ACS Appl. Mater. Interfaces* **2015**, *7*, 9831–9840. [[CrossRef](#)]
95. Su, H.; Wang, X.; Li, C.; Wang, Z.; Wu, Y.; Zhang, J.; Zhang, Y.; Zhao, C.; Wu, J.; Zheng, H. Enhanced Energy Harvesting Ability of Polydimethylsiloxane-BaTiO<sub>3</sub>-Based Flexible Piezoelectric Nanogenerator for Tactile Imitation Application. *Nano Energy* **2021**, *83*, 105809. [[CrossRef](#)]
96. Adhikary, P.; Garain, S.; Ram, S.; Mandal, D. Flexible Hybrid Eu<sup>3+</sup> Doped P(VDF-HFP) Nanocomposite Film Possess Hypersensitive Electronic Transitions and Piezoelectric Throughput. *J. Polym. Sci. B Polym. Phys.* **2016**, *54*, 2335–2345. [[CrossRef](#)]

97. Garain, S.; Jana, S.; Sinha, T.K.; Mandal, D. Design of in Situ Poled Ce<sup>3+</sup>-Doped Electrospun PVDF/Graphene Composite Nanofibers for Fabrication of Nanopressure Sensor and Ultrasensitive Acoustic Nanogenerator. *ACS Appl. Mater. Interfaces* **2016**, *8*, 4532–4540. [[CrossRef](#)]
98. Missaoui, S.; Bouhamed, A.; Khedri, M.H.; Khemakhem, H.; Kanoun, O. Enhanced piezoelectric performance of lead free BCZT based flexible nanogenerator. In Proceedings of the 18th IEEE International Multi-Conference on Systems, Signals and Devices, Monastir, Tunisia, 22–25 March 2021; pp. 889–894.
99. Shi, K.; Sun, B.; Huang, X.; Jiang, P. Synergistic Effect of Graphene Nanosheet and BaTiO<sub>3</sub> Nanoparticles on Performance Enhancement of Electrospun PVDF Nanofiber Mat for Flexible Piezoelectric Nanogenerators. *Nano Energy* **2018**, *52*, 153–162. [[CrossRef](#)]
100. Li, Y.; Tan, J.; Liang, K.; Li, Y.; Sun, J.; Zhang, H.; Luo, C.; Li, P.; Xu, J.; Jiang, H.; et al. Enhanced Piezoelectric Performance of Multi-Layered Flexible Polyvinylidene Fluoride–BaTiO<sub>3</sub>–RGO Films for Monitoring Human Body Motions. *J. Mater. Sci. Mater. Electron.* **2022**, *33*, 4291–4304. [[CrossRef](#)]
101. Luo, C.; Hu, S.; Xia, M.; Li, P.; Hu, J.; Li, G.; Jiang, H.; Zhang, W. A Flexible Lead-Free BaTiO<sub>3</sub>/PDMS/C Composite Nanogenerator as a Piezoelectric Energy Harvester. *Energy Technol.* **2018**, *6*, 922–927. [[CrossRef](#)]
102. Mandal, D.; Henkel, K.; Schmeißer, D. Improved Performance of a Polymer Nanogenerator Based on Silver Nanoparticles Doped Electrospun P(VDF-HFP) Nanofibers. *Phys. Chem. Chem. Phys.* **2014**, *16*, 10403–10407. [[CrossRef](#)] [[PubMed](#)]
103. Bera, B.; das Sarkar, M. Piezoelectricity in PVDF and PVDF Based Piezoelectric Nanogenerator: A Concept. *IOSR J. Appl. Phys.* **2017**, *9*, 95–99. [[CrossRef](#)]
104. Ye, S.; Cheng, C.; Chen, X.; Chen, X.; Shao, J.; Zhang, J.; Hu, H.; Tian, H.; Li, X.; Ma, L.; et al. High-Performance Piezoelectric Nanogenerator Based on Microstructured P(VDF-TrFE)/BNNTs Composite for Energy Harvesting and Radiation Protection in Space. *Nano Energy* **2019**, *60*, 701–714. [[CrossRef](#)]
105. Paria, S.; Karan, S.K.; Bera, R.; Das, A.K.; Maitra, A.; Khatua, B.B. A Facile Approach to Develop a Highly Stretchable PVC/ZnSnO<sub>3</sub> Piezoelectric Nanogenerator with High Output Power Generation for Powering Portable Electronic Devices. *Ind. Eng. Chem. Res.* **2016**, *55*, 10671–10680. [[CrossRef](#)]
106. Sriphan, S.; Charoonsuk, T.; Maluangnont, T.; Vittayakorn, N. High-Performance Hybridized Composites-Based Piezoelectric and Triboelectric Nanogenerators Based on BaTiO<sub>3</sub>/PDMS Composite Film Modified with TiO<sub>2</sub> Nanosheets and Silver Nanopowders Cofillers. *ACS Appl. Energy Mater.* **2019**, *2*, 3840–3850. [[CrossRef](#)]
107. Xia, M.; Luo, C.; Su, X.; Li, Y.; Li, P.; Hu, J.; Li, G.; Jiang, H.; Zhang, W. KNN/PDMS/C-Based Lead-Free Piezoelectric Composite Film for Flexible Nanogenerator. *J. Mater. Sci. Mater. Electron.* **2019**, *30*, 7558–7566. [[CrossRef](#)]
108. Qian, Y.; Kang, D.J. Poly(Dimethylsiloxane)/ZnO Nanoflakes/Three-Dimensional Graphene Heterostructures for High-Performance Flexible Energy Harvesters with Simultaneous Piezoelectric and Triboelectric Generation. *ACS Appl. Mater. Interfaces* **2018**, *10*, 32281–32288. [[CrossRef](#)]
109. Tripathy, A.; Maria Joseph Raj, N.P.; Saravanakumar, B.; Kim, S.J.; Ramadoss, A. Tuning of Highly Piezoelectric Bismuth Ferrite/PVDF-Copolymer Flexible Films for Efficient Energy Harvesting Performance. *J. Alloys Compd.* **2023**, *932*, 167569. [[CrossRef](#)]
110. Nour, E.S.; Sandberg, M.O.; Willander, M.; Nur, O. Handwriting Enabled Harvested Piezoelectric Power Using ZnO Nanowires/Polymer Composite on Paper Substrate. *Nano Energy* **2014**, *9*, 221–228. [[CrossRef](#)]
111. Huan, Y.; Zhang, X.; Song, J.; Zhao, Y.; Wei, T.; Zhang, G.; Wang, X. High-Performance Piezoelectric Composite Nanogenerator Based on Ag/(K,Na)NbO<sub>3</sub> Heterostructure. *Nano Energy* **2018**, *50*, 62–69. [[CrossRef](#)]
112. Yin, B.; Qiu, Y.; Zhang, H.; Lei, J.; Chang, Y.; Ji, J.; Luo, Y.; Zhao, Y.; Hu, L. Piezoelectric Performance Enhancement of ZnO Flexible Nanogenerator by a NiO-ZnO p-n Junction Formation. *Nano Energy* **2014**, *14*, 95–101. [[CrossRef](#)]
113. Liu, C.; Yu, A.; Peng, M.; Song, M.; Liu, W.; Zhang, Y.; Zhai, J. Improvement in the Piezoelectric Performance of a ZnO Nanogenerator by a Combination of Chemical Doping and Interfacial Modification. *J. Phys. Chem. C* **2016**, *120*, 6971–6977. [[CrossRef](#)]
114. Li, J.; Zhao, C.; Xia, K.; Liu, X.; Li, D.; Han, J. Enhanced Piezoelectric Output of the PVDF-TrFE/ZnO Flexible Piezoelectric Nanogenerator by Surface Modification. *Appl. Surf. Sci.* **2019**, *463*, 626–634. [[CrossRef](#)]
115. Zhang, C.; Fan, Y.; Li, H.; Li, Y.; Zhang, L.; Cao, S.; Kuang, S.; Zhao, Y.; Chen, A.; Zhu, G.; et al. Fully Rollable Lead-Free Poly(Vinylidene Fluoride)-Niobate-Based Nanogenerator with Ultra-Flexible Nano-Network Electrodes. *ACS Nano* **2018**, *12*, 4803–4811. [[CrossRef](#)]
116. Yang, C.; Song, S.; Chen, F.; Chen, N. Fabrication of PVDF/BaTiO<sub>3</sub>/CNT Piezoelectric Energy Harvesters with Bionic Balsa Wood Structures through 3D Printing and Supercritical Carbon Dioxide Foaming. *ACS Appl. Mater. Interfaces* **2021**, *13*, 41723–41734. [[CrossRef](#)] [[PubMed](#)]
117. Zhou, X.; Lee, P.S. Three Dimensional Printed Nanogenerators. *EcoMat* **2021**, *3*, e12098. [[CrossRef](#)]
118. Zhou, X.; Parida, K.; Halevi, O.; Liu, Y.; Xiong, J.; Magdassi, S.; Lee, P.S. All 3D-Printed Stretchable Piezoelectric Nanogenerator with Non-Protruding Kirigami Structure. *Nano Energy* **2020**, *72*, 104676. [[CrossRef](#)]
119. Li, H.; Lim, S. Screen Printing of Surface-Modified Barium Titanate/Polyvinylidene Fluoride Nanocomposites for High-Performance Flexible Piezoelectric Nanogenerators. *Nanomaterials* **2022**, *12*, 2910. [[CrossRef](#)]
120. Han, M.; Chen, X.; Yu, B.; Zhang, H. Coupling of Piezoelectric and Triboelectric Effects: From Theoretical Analysis to Experimental Verification. *Adv. Electron. Mater.* **2015**, *1*, 1500187. [[CrossRef](#)]

121. Mahmud, A.; Khan, A.A.; Islam, S.; Voss, P.; Ban, D. Integration of Organic/Inorganic Nanostructured Materials in a Hybrid Nanogenerator Enables Efficacious Energy Harvesting via Mutual Performance Enhancement. *Nano Energy* **2019**, *58*, 112–120. [[CrossRef](#)]
122. Patnam, H.; Dudem, B.; Alluri, N.R.; Mule, A.R.; Graham, S.A.; Kim, S.J.; Yu, J.S. Piezo/Triboelectric Hybrid Nanogenerators Based on Ca-Doped Barium Zirconate Titanate Embedded Composite Polymers for Wearable Electronics. *Compos. Sci. Technol.* **2020**, *188*, 107963. [[CrossRef](#)]
123. Patnam, H.; Graham, S.A.; Yu, J.S. Y-ZnO Microflowers Embedded Polymeric Composite Films to Enhance the Electrical Performance of Piezo/Tribo Hybrid Nanogenerators for Biomechanical Energy Harvesting and Sensing Applications. *ACS Sustain. Chem. Eng.* **2021**, *9*, 4600–4610. [[CrossRef](#)]
124. Yun, J.; Park, J.; Ryoo, M.; Kitchamsetti, N.; Goh, T.S.; Kim, D. Piezo-Triboelectric Hybridized Nanogenerator Embedding MXene Based Bifunctional Conductive Filler in Polymer Matrix for Boosting Electrical Power. *Nano Energy* **2023**, *105*, 108018. [[CrossRef](#)]
125. Zhang, K.; Wang, S.; Yang, Y. A One-Structure-Based Piezo-Tribo-Pyro-Photoelectric Effects Coupled Nanogenerator for Simultaneously Scavenging Mechanical, Thermal, and Solar Energies. *Adv. Energy Mater.* **2017**, *7*, 1601852. [[CrossRef](#)]
126. Ravikumar, R.; Natraj, V.; Sivalingam, Y.; Velappa Jayaraman, S.; Zheng, F.; Wang, H.; Du, Q.; Liu, N. Piezoelectric Nanogenerator Induced Work Function on Metal Phenolic Coordination Framework from Copper Oxide Nanosphere for Efficient Biomechanical Energy Harvesting and Physiological Monitoring. *J. Mater. Chem. C Mater.* **2022**, *10*, 16492–16505. [[CrossRef](#)]
127. Kappiarukudil, K.J.; Ramesh, M.V. Real-time monitoring and detection of “heart attack” using wireless sensor networks. In Proceedings of the 4th International Conference on Sensor Technologies and Applications, Venice/Mestre, Italy, 18–25 July 2010; pp. 632–636.
128. Rana, M.M.; Khan, A.A.; Huang, G.; Mei, N.; Saritas, R.; Wen, B.; Zhang, S.; Voss, P.; Abdel-Rahman, E.; Leonenko, Z.; et al. Porosity Modulated High-Performance Piezoelectric Nanogenerator Based on Organic/Inorganic Nanomaterials for Self-Powered Structural Health Monitoring. *ACS Appl. Mater. Interfaces* **2020**, *12*, 47503–47512. [[CrossRef](#)]
129. Wu, P.; Chen, P.; Xu, C.; Wang, Q.; Zhang, F.; Yang, K.; Jiang, W.; Feng, J.; Luo, Z. Ultrasound-Driven in Vivo Electrical Stimulation Based on Biodegradable Piezoelectric Nanogenerators for Enhancing and Monitoring the Nerve Tissue Repair. *Nano Energy* **2022**, *102*, 107707. [[CrossRef](#)]
130. Azimi, S.; Golabchi, A.; Nekookar, A.; Rabbani, S.; Amiri, M.H.; Asadi, K.; Abolhasani, M.M. Self-Powered Cardiac Pacemaker by Piezoelectric Polymer Nanogenerator Implant. *Nano Energy* **2021**, *83*, 105781. [[CrossRef](#)]
131. Sharma, A.; Panwar, V.; Mondal, B.; Prasher, D.; Bera, M.K.; Thomas, J.; Kumar, A.; Kamboj, N.; Mandal, D.; Ghosh, D. Electrical Stimulation Induced by a Piezo-Driven Triboelectric Nanogenerator and Electroactive Hydrogel Composite, Accelerate Wound Repair. *Nano Energy* **2022**, *99*, 107419. [[CrossRef](#)]

**Disclaimer/Publisher’s Note:** The statements, opinions and data contained in all publications are solely those of the individual author(s) and contributor(s) and not of MDPI and/or the editor(s). MDPI and/or the editor(s) disclaim responsibility for any injury to people or property resulting from any ideas, methods, instructions or products referred to in the content.